Politecnico di Milano

V Facoltà di Ingegneria

Corso di laurea in Ingegneria delle Telecomunicazioni

Dipartimento di Elettronica, Informazione e Bioingegneria

Atmospheric phase screen estimation by means of a geosynchronous synthetic aperture radar

Supervisor: Prof. Andrea Monti Guarnieri

Thesis by:

Zeno Romano

Student ID 798163

Session 2013 - 2014

Ringraziamenti

Ci sono molte persone che devo ringraziare per il supporto dato durante il mio percorso universitario e lo sviluppo di questa tesi.
Prima di tutto un grazie alle persone a cui devo tutto ciò che ho ottenuto, ai miei genitori, per un sostegno morale ed economico senza il quale non avrei mai potuto completare gli studi e raggiungere questo importante traguardo.
Grazie al Prof. Monti Guarnieri, per avermi proposto un argomento molto interessante e per avermi seguito nello sviluppo di questa tesi, e grazie anche ad Andrea Recchia per avermi seguito in questo periodo.
Grazie ai miei zii e ai miei cugini che mi hanno ospitato per alcuni anni in casa e mi hanno reso molto piacevole il mio periodo di studi a Milano.
Grazie a mia nonna per il sostegno fornitomi e che negli ultimi mesi mi ha permesso di usare casa sua come mia sala studio.
Grazie agli amici che mi sono stati vicini in questo periodo.

Contents

Abstract **8**

Sommario **9**

1 Introduction **10**

1.1 Synthetic Aperture Radar 10

1.2 GEOSAR 14

1.3 Decorrelation sources 16

1.4 Purpose of the thesis 19

1.5 Related Works 19

2 Model and data acquisition **23**

2.1 GEOSAR system 23

2.2 Atmospheric phase screen 24

2.3 Acquisition model and APS effects 27

2.4 Model for APS estimation 29

2.5 Phase model for APS estimation 34

2.6 Power budget 35

3 APS estimation through MMSE estimator **37**

3.1 Ideal case: only APS 37

3.2 Average and MMSE estimator 41

4 APS estimation through SVD **47**

4.1 Ideal case: known scene 50

4.1.1 Improvement in the estimate using multi-look 53

4.2 One Permanent Scatterer per area 54

4.3 Only one Permanent scatterer in the whole scene known 56

5 APS estimation through ML estimator **59**

6 Comparison of estimators **66**

7 Conclusions **68**

Appendix A **69**

Appendix B **71**

Appendix C **75**

List of Figures

1.1 SAR geometry 11
1.2 GEOSAR system 14
1.3 Elliptic trajectory 16

2.1 GEOSAR, TLCOMP system 23
2.2 Example of APS 26
2.3 Azimuth resolution in L and X-band 28
2.4 Example of Stack 30
2.5 APS in L and X bands 33

3.1 MMSE: APS estimation with known scene 39
3.2 MMSE: RMSE with known scene 39
3.3 MMSE: RMSE with known scene, splitting the image 41
3.4 MMSE: Scene average 42
3.5 MMSE: Estimate of the APS with average estimator 44
3.6 MMSE: RMSE of the estimate of the APS with average estimator 45
3.7 MMSE: RMSE of the estimate of the APS splitting the scene . . . 46

4.1 SVD: APS estimate with high SNR 48
4.2 SVD: APS with known scene 52
4.3 SVD: RMSE with known scene 52
4.4 SVD: average over an area 53

4.5 SVD: RMSE averaging over an area 54
4.6 SVD: 1 PS per area 55
4.7 SVD: RMSE knowing 1 PS per area 56
4.8 SVD: Estimate of the APS with one PS 57
4.9 SVD: RMSE knowing only 1 PS 58

5.1 MLE: Estimate of the APS 62
5.2 MLE: RMSE vs iterations 62
5.3 MLE: Estimate of the APS with spatial filter 64
5.4 MLE: RMSE vs iterations with spatial filter 64
5.5 MLE: RMSE vs SNR 65

6.1 Comparison of different estimators 67

List of Tables

1.1 GEOSAR systems 15
1.2 GEOSAR technical characteristics 15

2.1 L-band vs X-band 24
2.2 Working conditions 36

Abstract

There are many Low Earth Orbit SAR (LEOSAR) satellite orbiting around the Earth that are used to monitor the planet. These satellites perform really well for certain applications, but present some limits (mainly due to their high revisit time) for other purposes.

Recently solutions involving Geosynchronous Synthetic Aperture Radar (GEOSAR) systems have been proposed, but never implemented due to decorrelation issues in the images. One of the most important decorrelation sources is the Atmospheric Phase Screen (APS) originated in the troposhere.

This thesis will present few algorithms to estimate the APS seen with a GEOSAR system.

At first the geometry, parameters and the technical requirements of the system are shown. The data acquisition process is presented along with the generation of the stack of images and the model, these will be used as data to be processed. Then three methods to estimate the APS are proposed starting from the stack. Each method will be introduce with strong assumptions that will be later removed to move into a more realistic scenario.

In the end results of the simulations and a comparison of the three methods are shown.

Sommario

Ci sono molti satelliti Low Earth Orbit SAR (LEOSAR) che orbitano attorno alla Terra per monitorare il pianeta. Questi satelliti si comportano in certe applicazioni, ma presentano dei limiti per altri scopi (principalmente dovuti al tempo di rivisita).

Recentemente, sono state proposte delle soluzioni che richiedevano l'uso di SAR in orbita geosincrona, ma non sono mai stati implementati a causa di problemi di decorrelazione nelle immagini. Una delle più importanti sorgenti di decorrelazione è lo Schermo Atmosferico di Fase (APS) che ha origini nella troposfera.

Questa tesi presenterà alcuni algoritmi per stimare l'APS vista con un sistema GEOSAR.

All'inizio verranno mostrati la geometria, i parametri e i requisiti tecnici del sistema. Sarà presentato il processo di acquisizione dei dati e la generazione dello stack di immagini che verranno utilizzati per la stima.

Poi verranno proposti tre metodi per la stima dell'APS. Ogni algoritmo sarà introdotto partendo da forti supposizioni che verranno successivamente rimosse per mostrare uno scenario più realistico.

Alla fine ci sarà un confronto tra i risultati ottenuti nelle simulazioni con i vari metodi.

Chapter 1

Introduction

Since 1957 when the Soviet Union launched Sputnik 1 in space, mankind has been working hard in order to exploit satellites to communicate and monitor the Earth, and in 1978 Seasat was the first satellite that had on board a spacebourne synthetic aperture radar (SAR).

1.1 Synthetic Aperture Radar

A SAR system is a radar that is designed to achieve high resolution and coherent images of the Earth.

It exploits microwaves in order to obtain some useful features[1]: the penetration of clouds and also foliage if longer wavelength are utilized, the sensitivity to surface roughness, the use of phase for target location and motion identifications.

The SAR is a radar mounted on a satellite or an airplane in order to mimic the behaviour of a big array of antennas, this array simulates a wide-aperture discrete antenna. Many low-resolution observations are obtained by the sensor during its motion and then combined together to realize a high resolution image.

The geometry of a SAR is depicted in fig. 1.1, the antenna is not pointed directly

beneath the satellite, this is done to avoid the left-right ambiguity, the sensor records the time interval between the transmission of the signal and the reception of a replica scattered back from a target, but can not distinguish the direction. In the picture θ_L and θ_I are the "look angle" and the "incidence angle" respectively, notice that for a satellite borne SAR $\theta_L \neq \theta_I$ due to the Earth curvature ($\theta_L < \theta_I$). The incidence angle is usually between 20 and 50 degrees.

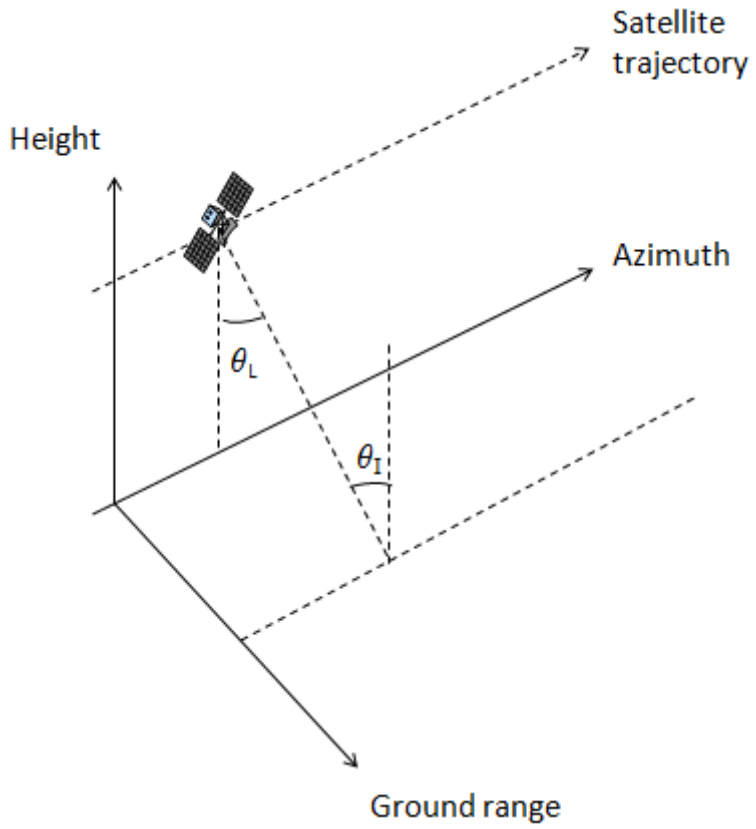

Figure 1.1: SAR geometry

Most SAR systems use microwaves in the bands between L and X.

The L-band (from 1 GHz to 2 GHz) is a lower limit because longer wavelength would require large antennas and would not allow to use large bandwidth, and a small bandwidth yields a coarse resolution.

The X-band (from 8 GHz to 12 GHz) is an upper limit because frequencies above 10 GHz are strongly attenuated by rain and clouds.

The L-band can penetrate the tree cover but higher frequencies are more sensitive to motion and allow higher resolution.

The SAR is only capable of performing a 2D acquisition, it will sense every target at the same distance as a single one. In order to see the third dimension we need additional information like another SAR travelling on a parallel track, or a DEM (digital elevation model, topology of the observed area).

In term of resolution, using a SAR we can get a very high resolution in range, the slant range resolution depends only on the used bandwidth B

$$\rho_r = \frac{c}{2B} \tag{1.1}$$

that we can convert to ground resolution knowing the incidence angle

$$\rho_g = \frac{\rho_r}{\sin(\theta_I)} = \frac{c}{2B\sin(\theta_I)} \tag{1.2}$$

The azimuth resolution is very high if we synthetize a very wide-aperture antenna using many observations

$$\rho_{az} = \frac{\lambda}{2L_s} r_0 \tag{1.3}$$

where r_0 is the slant range (distance between satellite and target) and L_s is the length of the synthetic aperture that depends on the velocity of the satellite (or airplane) v and the integration time T ($L_s = vT$), so we can also write the azimuth resolution in the following way

$$\rho_{az} = \frac{\lambda}{2vT} r_0 \tag{1.4}$$

For an antenna with a physical size L_a the angular aperture is

$$\Delta\psi = \frac{\lambda}{L_a} \tag{1.5}$$

This aperture will limit the synthetic aperture since a target would not be visible for an interval wider than $\Delta\psi$. Therefore the sinthetic length is at most

$$L_s < r_0 \Delta\psi = r_0 \frac{\lambda}{L_a} \tag{1.6}$$

and this gives a limit in the azimuth resolution that depends on size of the antenna

$$\rho_{az} = \frac{\lambda}{2 r_0 \frac{\lambda}{L_a}} r_0 = \frac{L_a}{2} \tag{1.7}$$

Equation 1.7 shows that the azimuth resolution improves with smaller antennas, because that corresponds to a wider angle aperture and therefore to a possible wider synthetic aperture.

Spaceborne SAR systems have been used and are still used on Low Earth Orbit (LEO) satellites (at an altitude of about 800 Km).
Their main applications are: enviromental monitoring (especially for natural disaster), DEM generation, military surveillance.
An example of working LEOSAR is the Italian Space Agency's COSMO-SkyMed whose applications[2] are: monitoring and preventions of natural disasters, coastline monitoring (erosion and pollution), agricoltural monitoring, urban monitoring of buildings (subsidence of the ground) and accurate cartography; an other example is the European Space Agency's Sentinel-1 whose applications[3] are: monitoring of sea-ice zones, monitoring of movements and mapping of Earth surface and mapping of natural disaster for emergency response.
LEOSAR systems perform really well for certain applications and have a coverage of all the Earth surface, but have an important drawback for other purposes, their revisit time is quite high, therefore it will take few days to look at the same section of the world, this mean that processes with short timescales are difficult to be measured.

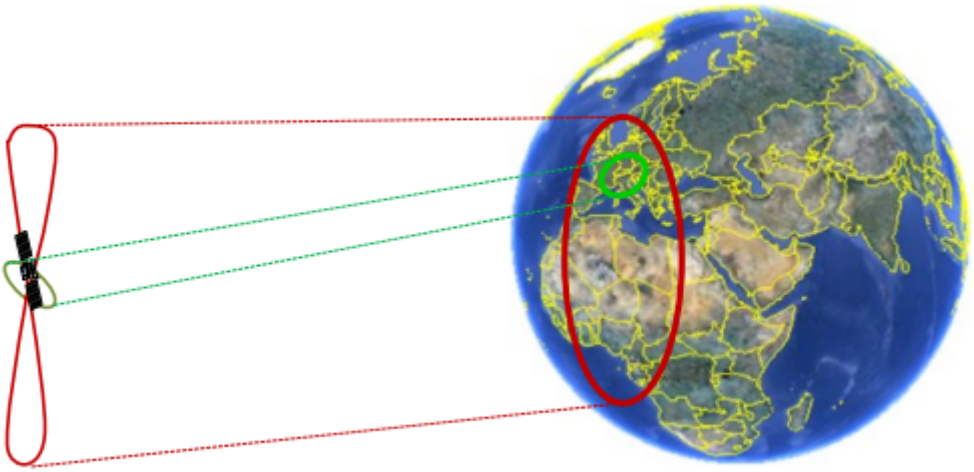

Figure 1.2: GEOSAR system acquisition geometry, red lines representing a continental GEOSAR, green lines representing a regional GEOSAR

1.2 GEOSAR

A possible solution in term of better revisit time is to place a satellite on a geosynchronous orbit, this means that the satellite would stay at the altitude of a geostationary satellite (about 36000 Km) while travelling on an ellipse or an eight-shape trajectory in one day, as illustrated in fig. 1.2.

As shown in fig. 1.2 there are two proposed SAR systems that have been presented to work on a geosynchronous orbit, the first one is a continental system (introduced by Tomiyasu in 1978 [4]) and the second one called TeLecom COMPatible (TLCOMP) that can cover a regional area (Prati, Rocca, Giancola, Monti 1998). Characteristics of the two GEOSAR systems and a comparison with the LEOSAR are shown in the following table

	Continental	**TLCOMP**	**LEOSAR**
Coverage	Continental	Regional	World
Integration time	Few minutes	Few minutes - 7 hours	<1 second
Atmosphere	Almost frozen	Sensed, to be compensated	Frozen
Line of sight	East-West	North-South	East-West
Revisit time	Once a day	Twice a day	Few days

Table 1.1: Characteristics of two GEOSAR systems and a LEOSAR

Looking at the last table we can notice that a LEOSAR has a very low integration time because thanks to its high speed (about 8 Km/s) and that means a very wide-aperture in less than a second and therefore a good resolution, but has a very low revisit time if we compare it to the GEOSAR systems.
If we now focus only on the GEOSAR systems, we can see the technical characteristics of the two systems shown in table 1.2.

	Continental	**TLCOMP**
Antenna diameter	15-30 m	3-6 m
Average P_T	3000 W	400 W
PRF	200 Hz	50 Hz
Velocity at equator	1100 m/s	5 m/s

Table 1.2: Characteristics of two GEOSAR systems

Although many GEOSAR concepts have been proposed, none of them has been implemented because of technological constraints, as we can see in table 1.2 the continental GEOSAR would require a very big antenna and a really high transmission power. The TLCOMP is actually feasible and this is the reason why from now on we will consider only this system, but due to the higher integration time it will suffer from a decorrelation problem (discussed later).
The TLCOMP requires the satellite to travel on an elliptic trajectory in one day

and to revisit the same orbit in consecutive days. In order to obtain a good azimuth resolution we would need large synthetic apertures, therefore the SAR acquisition will be performed in the sections of the ellipse with lower curvature (fig. 1.3). This gives us two integration time of about 8 hours per day.

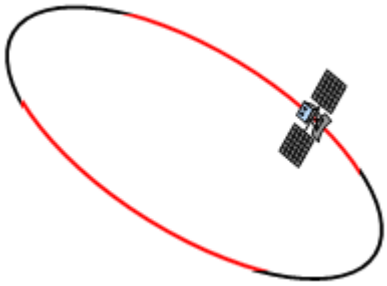

Figure 1.3: The red sections of the elliptic trajectory will be used for synthetic apertures

1.3 Decorrelation sources

The main challenges for a GEOSAR come from the long range from a geostationary orbit to the Earth surface, so scattered signals are weak and high power, large antennas or long integration times are needed. With a high integration time the targets and the atmosphere may be affected by temporal decorrelation and this might prevent aperture synthesis (or at least deteriorate the resolution of the images).

There are many factors that generates decorrelation in the images. Sometimes we can compensate for this effect and prevent that some of the energy scattered back from a target would spread on nearby targets, causing defocusing and blurring in the images. In other cases we can not compensate for the decorrelation, the only thing we can do is to evaluate how much the image will be deteriorated.

One source of decorrelation is **scene decorrelation** (or clutter decorrelation), that is due to a target motion.

If we consider a displacement of a target during the integration time, the SAR

sees a displacement in the slant range that generates a phase distortion [5] and the energy of the reflection would spread on a bigger area, this may cause a loss of azimuth resolution.

The targets that generate this decorrelation are objects that moves during the integration time (for example leaves blown by the wind), some of these targets can be filter out by a GEOSAR that uses frequencies in the L-band (it may be able to see the ground through the tree tops). Varying integration time (and the resolution), different noise sources might be filtered out; this could help estimating the effect of some decorrelation sources like the vegetations or the ionosphere.

Another source of decorrelation are the **Earth tides**, solid Earth has tides and the surface slightly moves due to the gravity attraction by the Moon and the Sun. There are three different relevant processes:

- Solid Earth tides: this is the biggest contributor to Earth tidal displacement, it has a period of 12 hours and an amplitude comparable with λ and needs to be compensated. There are models to estimate this displacement with an accuracy of 1 mm, the residual error can be considered as gaussian noise and will give a performace loss of about 0.01 dB;

- Ocean loadings: this effect has an amplitude of few centimeters, there are models that can compensate this effect with an accuracy of 3 mm, if we consider the error as gaussian noise the performance loss would be 0.15 dB;

- Pole tides: this is the response of the ocean to the variations of the centrifugal force due to wobbling of the Earth's rotational axis. Ita has a periods of 12 and 14 months so displacement generated during the integration time can be neglected.

Another source of decorrelation is the **Ionospheric delay**, the ionosphere causes a delay in the SAR pulses that means an advance in the received signal that is

proportional to the total electon content (TEC) and inversely proportional to the frequency

$$\delta_\phi = -\frac{2\pi}{c_0}\frac{40.28}{f}TEC \tag{1.8}$$

since the TEC can vary in a 8-hour integration time, this phase shift needs to be compensated. There are two types of decorrelation: spatial decorrelation (different points of the ionosphere have different TEC) and temporal decorrelation (the TEC changes with time). Both of this issues can be solved using sub-aperture focusing, this implies many windows with a shorter integration time (few minutes) in which the ionosphere can be considered still, and using a GEOSAR, the synthetic aperture projected on the ionospheric layer (altitude of about 400 Km) is only few Km where we can consider the ionosphere to be constant.

The last source of decorrelation is the **Tropospheric delay**, it is caused by local eterogeneities in the air's refractive index n in the troposphere (lower layer of the atmosphere) that induce variations in the slant path from the target to the satellite. This delay can be divided in two main components: hydrostatic and wet delays.

$$(n-1)\,10^6 = \frac{77.6P}{T} + \frac{3.73\cdot 10^5 e}{T^2} \tag{1.9}$$

Where n is the refrective index, P the pressure measured in millibars, T the temperature in Kelvin and e is the water vapor pressure in millibars.

The hydrostatic delay depends on pressure and temperature, while the wet component is caused by the water vapor (humidity) in the air, it is usually smaller than the hydrostatic one but much more variable and thus harder to remove; it needs to be compensated before focusing to obtain a good resolution. It is a zero mean gaussian process that introduces a random phase term that is called Atmospheric Phase Screen (APS).

1.4 Purpose of the thesis

We have just introduced the Atmospheric Phase Screen, that is generated in the troposphere by the humidity in the air; this effect needs to be compensated, especially if high integration times are used, otherwise the APS will add a random component in the phases of the targets that will cause defocusing in the scene and blurring in the SAR images.
The purpose of this thesis is to present three different algorithms that should be able to estimate the atmospheric phase screen starting from images taken over many days.
Estimating the APS is a crucial point because this is one of the main problems that have prevented the implementation of GEOSAR systems.
Implementing a TLCOMP system would allow us to realize the following applications:

- real time monitoring of events like landslides, motion of glaciers and volcanoes [6] and building deformations in urban areas;
- generation of 3D ground subsidence map, combining TLCOMP and LEOSAR data [7].
- generation of water vapor maps [8] (humidity in the atmosphere);

A LEOSAR system would be capable to realize the first two applications, but not in real time, while a GEOSAR is always looking at the same area and would be able to notice any sudden change of the surface of the Earth.

1.5 Related Works

There have been studies on the estimate of the delay introduced by the atmosphere.

There are models that use meteorological data (temperature, pressure and humidity) acquired at ground stations. Among these, the most common are the Hopfield, Saastamoinen and EGNOS model [9].

In the Hopfield model the temperature is assumed to fall at a rate of $\beta = -6.5°C/Km$ going up, the zenith atmospheric delay will be

$$d = 10^{-6} k_1 \frac{P_0}{T_0} \frac{H_d - h}{5} + 10^{-6} \left[k_3 + 273(k_2 - k_1)\right] \frac{e_0}{T_0^2} \frac{H_w - h}{5} \tag{1.10}$$

Where $H_d = 40136{+}148.72(T_0{-}273.15)\ m$ and $H_w = 11000\ m$ are the height of the dry and wet atmospheric layer, P_0 is the ground pressure $(mbar)$, T_0 the ground temperature $(°C)$, e_0 the ground water vapor pressure (mbar) and h the height of the observation station. There are three constant parameters $k_1 = 77.6\ K/mbar$, $k_2 = 71.6\ K^2/mbar$ and $k_3 = 3.737 \times 10^5\ K^2/mbar$.

The Saastamoinen model once again consider a constant rate of change of the atmosphere of $\beta = -6.5°C/Km$ going up from the observation station. The delay is modelled as

$$d = 0.002277 \frac{P_0 + \left(0.05 + \frac{1255}{T_0 + 273.15}\right) e_0}{f(\varphi, h)} \tag{1.11}$$

with

$$\begin{cases} e_0 = rh \times 6.11 \times 10^{\frac{7.5 T_0}{T_0 + 273.15}} \\ f(\varphi, h) = 1 - 0.00266 \cos(2\varphi) - 0.00028 h \end{cases}$$

where rh is the relative humidity (between 0 and 1), $f(\varphi, h)$ is the modification of the variation in the gravitational acceleration caused by the Earth rotation and φ and h are the geocentric latitude (°) and geodetic height (Km) of the observing station respectively.

The EGNOS (European Geostationary Navigation Overly System) model divides the dry and wet components of the troposphere

$$d_{dry} = \frac{10^{-6} k_1 R_d p}{g_m} \left(1 - \frac{\beta H}{T}\right)^{\frac{g}{\beta R_d}} \tag{1.12}$$

$$d_{wet} = \frac{10^{-6} k_2 R_d}{g_m(\mu + 1) - \beta R_d} \frac{e}{T} \left(1 - \frac{\beta H}{T}\right)^{\frac{(\mu+1)g}{\beta R_d} - 1} \tag{1.13}$$

where $g = 9.80665\ m/s^2$, $g_m = 9.784\ m/s^2$, $R_d = 287.054\ J/K/Kg$, H is the height of a receiver above sea level (m), T the temperature (K), e is the water vapor pressure$(mbar)$, p is the atmospheric pressure $(mbar)$, β the change rate of the temperature (K/m), μ is the change rate of the water vapor (dimensionless), $k_1 = 77.604\ K/mbar$ and $k_2 = 382000\ K^2/mbar$.

Using radars, a method to estimate the APS by means of a ground-based radar has been presented [10], and tests have been carried out. The main idea is to look for the difference in the received phase from a stable target (ground control point) in consecutive images, since the target is still the phase variations are due to the atmospheric phase screen, this method can be improved exploiting data obtained from a nearby meteo station to tune the humidity (looking to maximize the average coherence of stable targets in consecutive images) and get an estimate of the refractive index that leads to a first estimate of the delay introduced by the APS.

Hobbs presented a method to track APS variations in time with a GEOSAR [11]. If the rate of change of the APS is linear this causes an azimuth shift that is proportional to the rate of change, deviations from linearity causes defocusing in the image. This fact provides an opportunity to track the variation of the APS of a pixel (or a group of pixels) using consecutive images taken with short integration times and looking at the azimuth displacements of a target in those images. This method requires to use only integration times short enough that we can approximate the changes in time as linear.

Another method presented for the estimation of the APS using a GEOSAR system

looks for stable point targets. This scatterers should ideally present a constant phase over time and the phase variations are due to the effect of the APS, in this way we can estimate the atmospheric phase screen over this scatterers. If we have many stable point targets (like in urban areas) we can get a grid of values of the APS. Then if we use a temporal and 2-D cubic interpolation we can obtain the continuous phase screen in time and space [12].

Chapter 2

Model and data acquisition

2.1 GEOSAR system

From now on we will focus only on the GEOSAR based on the TLCOMP system using frequencies between the L and X-band (for the reasons stated in the previous chapter).

Fig. 2.1 shows an example of a TLCOMP and introduces the differences in coverage at different bands.

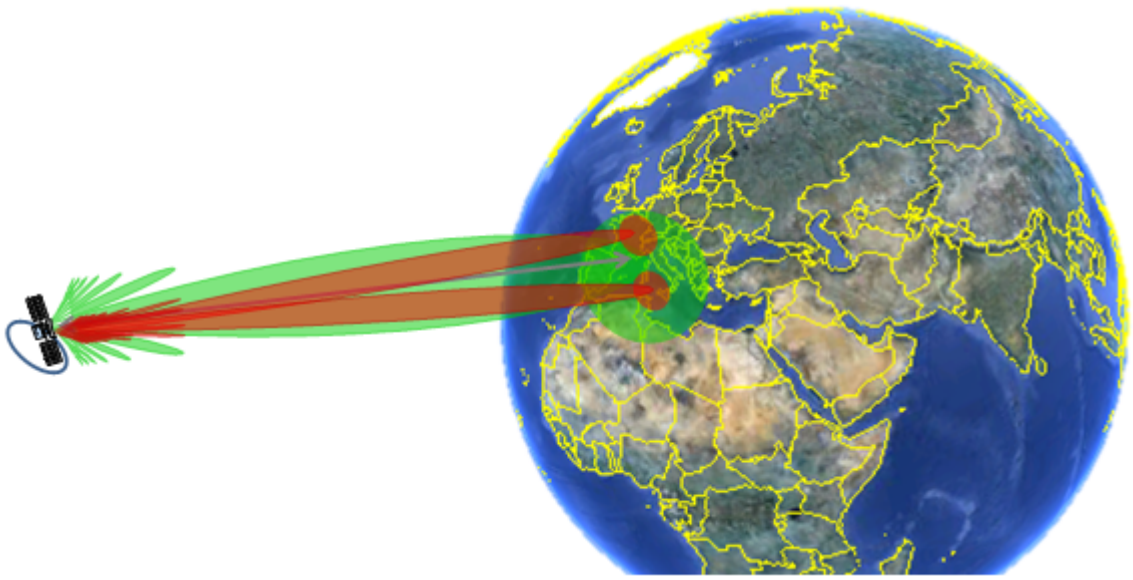

Figure 2.1: GEOSAR system; L-band (green ray), X-band (red rays)

The main differences between the to working frequencies are shown in the following table

	L-band	X-band
Coverage	3000 Km	300 Km
Resolution	Coarse (50 m × 50 m)	Fine (10 m × 10 m)
Effect of vegetation	Penetration over vegetation	Decorrelation of vegetation
Effect of clutter decorrelation	Less affected	Highly affected
Troposphere effect	Fairly affected	Highly affected
Ionosphere effect	Fairly affected	Not affected

Table 2.1: Main differences between L and X-band in a GEOSAR system

Different applications may require to use different bands, but they all be affected by the atmospheric phase screen, especially if long integration times are used in order to achieve better azimuth resolution.

2.2 Atmospheric phase screen

The atmospheric phase screen is a zero mean random process d_{APS} (measured in millimeters) that depends on the humidity in the troposphere.
It is a 4D process (3D in space and the time dimension) and given a short enough time interval (where we can consider no variations of the APS in time) a GEOSAR should be able to sense a 2D APS (range and azimuth directions).
According to [13] we can describe the APS with its variogram

$$2V(t_1, t_2) = var[d(t_1) - d(t_2)] = E\left[|d(t_1) - d(t_2)|^2\right] \tag{2.1}$$

the APS is a stationary process and if we consider τ as the difference between t_1

and t_2 we can write the variogram as

$$2V(\tau) = E\left[|d(t+\tau) - d(t)|^2\right] = 2\sigma_t^2\left(1 - e^{-\sqrt{\left(\frac{\tau}{\tau_0}\right)^2}}\right) \tag{2.2}$$

where σ_t^2 is the power of the process and τ_0 is the decorrelation time.

Usually σ_t^2 assumes value around 400 mm^2 (average atmosphere) and can get as low as 200 mm^2 (weak atmosphere) and as high as 1000 mm^2 (strong atmosphere). The decorrelation time is usually around 10 hours.

From the variogram we can also derive the autocorrelation function $r(\tau)$ knowing that

$$r(\tau) = \sigma_t^2 - \frac{2V(\tau)}{2} \tag{2.3}$$

we get

$$r(\tau) = \sigma_t^2 - \sigma_t^2\left(1 - e^{-\sqrt{\left(\frac{\tau}{\tau_0}\right)^2}}\right) = \sigma_t^2 e^{-\left|\frac{\tau}{\tau_0}\right|}. \tag{2.4}$$

These variogram and autocorrelation function depend only on time, but with similar steps we can add the space dependence. From

$$2V(\tau,\chi) = var\left[|d(t+\tau, x+\chi) - d(t,x)|^2\right] \tag{2.5}$$

we will get the following variogram and autocorrelation

$$2V(\tau,\chi) = 2\sigma_{t,x}^2\left(1 - e^{-\sqrt{\left(\frac{\tau}{\tau_0}\right)^2+\left(\frac{\chi}{\chi_0}\right)^2}}\right) \tag{2.6}$$

$$r(\tau,\chi) = \sigma_{t,x}^2 e^{-\sqrt{\left(\frac{\tau}{\tau_0}\right)^2+\left(\frac{\chi}{\chi_0}\right)^2}} \tag{2.7}$$

where χ_0 is the decorrelation space (usually between 10 and 20 km).

An example of an APS is shown in fig. 2.2.

Until now we have considered the atmospheric phase screen d_{APS} in millimeters,

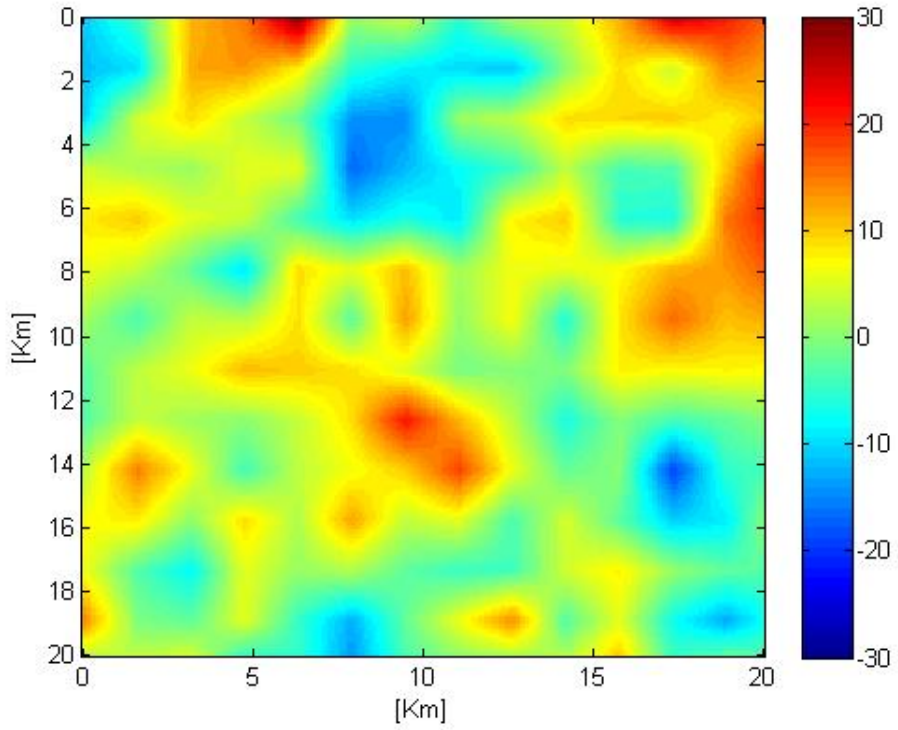

Figure 2.2: An example of an atmospheric phase screen shown in millimeters.

this translates to a phase term ϕ_{APS} that depends on the frequency (or wavelength λ) used

$$e^{j\frac{4\pi}{\lambda}d_{APS}} = e^{j\phi_{APS}} \tag{2.8}$$

This phase term will have a slightly different autocorrelation function (steps to obtain it are in appendix A)

$$r_{\phi}(\tau) = e^{-\left(\frac{4\pi}{\lambda}\right)^2 \sigma_t^2 \left|\frac{\tau}{\tau_0}\right|} \tag{2.9}$$

where we can also add the space dependence

$$r_{\phi}(\tau, \chi) = e^{-\left(\frac{4\pi}{\lambda}\right)^2 \sigma_t^2 \sqrt{\left(\frac{\tau}{\tau_0}\right)^2 + \left(\frac{\chi}{\chi_0}\right)^2}} \tag{2.10}$$

2.3 Acquisition model and APS effects

According to [14] in order to evaluate the impact of the atmospheric phase screen on a GEOSAR acquisition, we have to start from the GEOSAR impulse response function (IRF) in presence of the APS

$$h(t,\tau,\boldsymbol{P}) = w(\tau,\boldsymbol{P})g\left(t-\frac{R(\tau,\boldsymbol{P})}{2c}\right)exp\left(-j\frac{4\pi}{\lambda}R(\tau,\boldsymbol{P})\right)exp\left(-j\frac{4\pi}{\lambda}d_{APS}(\tau,\boldsymbol{P})\right) \tag{2.11}$$

where t is the fast time, τ is the slow time and $\boldsymbol{P}$ is the 3D location of the target, there are four terms in the last equation: the first is the slow amplitude change due to the antenna pattern and the spread losses, the second is the delayed version of the transmitted pulse, the third is the phase term due to the sensor-to-target distance variation and the fourth is the phase distortion introduced by the APS. Starting from equation 2.9 we can compute the power spectrum of the APS process

$$S_{APS}(f,T) = \frac{2}{k(T)}\frac{1}{1+\frac{(2\pi f)^2}{k(T)^2}} \tag{2.12}$$

with

$$k(T) = \frac{\sigma_{\tau,\chi}^2 T}{\tau_0^2}\left(\frac{4\pi}{\lambda}\right)^2 \tag{2.13}$$

From equation 2.12 we may notice that the power spectrum of the APS depends on the observation time T, the longer the integration time the more dispersed the resulting APS power spectrum.

If we try to focus an image without compensating for the APS, the resulting image would be the convolution between the GEOSAR azimuth IRF and the spectrum of the APS at the time of the acquisition.

Thanks to this convolution the energy of the targets will spread through the image

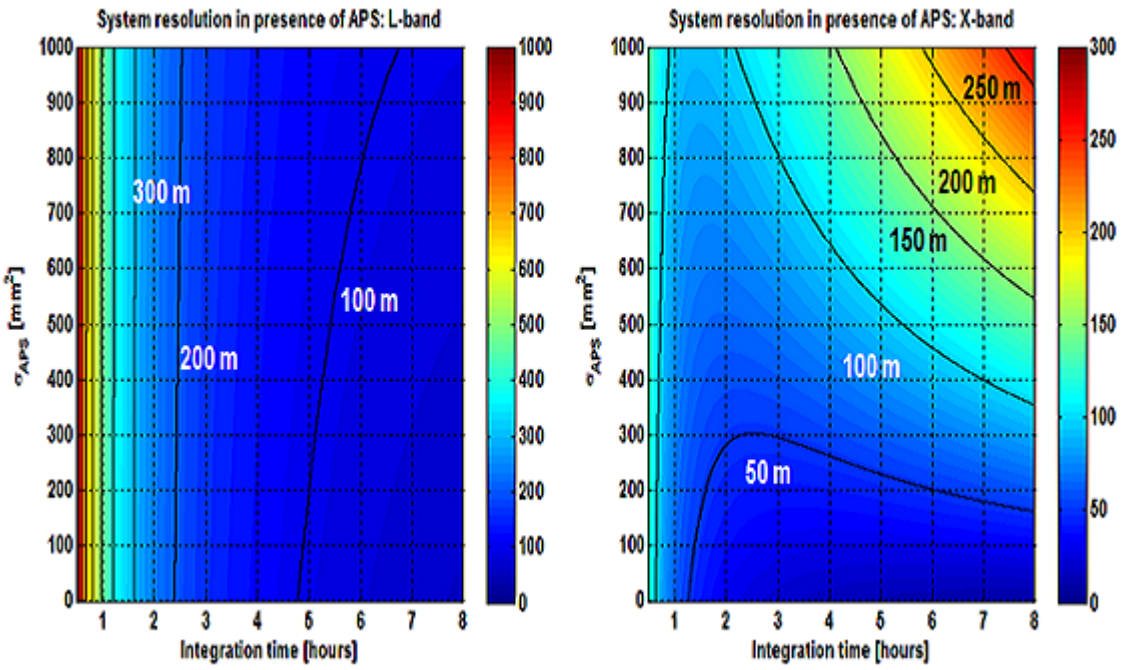

Figure 2.3: Azimuth resolution in L-band (left) and X-band (right)

causing a loss of resolution in the azimuth direction.

We stated in equation 1.4 that the SAR azimuth resolution is

$$\rho_{az,SAR} = \frac{\lambda}{2vT} r_o \tag{2.14}$$

the final resolution can be approximated as the summation between $\rho_{az,SAR}$ and the FWHM (full width at half maximum) of the APS process power spectrum shown in equation 2.12

$$\rho_{az} = \rho_{az,SAR} + \rho_{APS,SAR} = \left(\frac{\lambda}{2vT} + \frac{8\pi T \sigma^2_{\tau,\chi}}{v\tau_0^2 \lambda} \right) r_0 \tag{2.15}$$

Fig. 2.3 shows the azimuth resolution (as a function of the integration time, and APS power) for L and X-band GEOSAR systems. It can be noticed that the resolution is slightly impacted by the APS power for an L-band system, while a high APS power has a big impact on the resolution of an X-band GEOSAR.

If we were able to accurate estimate the APS, we could compensate for it and

achieve the resolution shown in equation 2.14, so we could obtain better focused SAR images.

2.4 Model for APS estimation

Although we would like to have a long integration time to achieve a good azimuth resolution, we need to use a time window where the APS can be considered still, that's why we should split the total time into many shorter integration times (sub-apertures) to get many images per day. In this way we can track the variations in the APS.

Looking at equation 2.15 we may notice that the resolution depends on T, the first term indicates that we need a long integration time, the second one that we need a short T in order to achieve a good resolution. There is a minimum around 15 to 20 minutes, and in that time interval we can also consider the APS to be still, therefore we should use integration times of about 15 to 20 minutes, and we will get 3 to 4 images per hour.

One image is not enough to get an estimate of the APS, beacause we would have more unknowns (ground reflectivity and APS) than data. Consecutive images would look at the same area but from a different sub-aperture (different incidence angle means a different perceived ground reflectivity) and would be affected by an other APS, so we can not combine the informations from consecutive images to estimate the APS because they would not sense the same scene and atmosphere. In order to solve this problem we have to exploit the revisit time of the satellite that every day comes back on the same orbit and can perform SAR acquisitions from the same sub-apertures.

When the satellite looks at the Earth from the same sub-aperture, but in different days, it should sense the same ground complex reflectivity (it will be slightly changed due to temporal decorrelation) and a completely different APS.

We can exploit the fact that the scene should remain almost unchanged in consecutive days to process the received data to remove the scene from the images, and that should yield us the atmospheric phase screen.

We need a "Stack of images", it is a collection of SAR acquisitions that creates a table of images taken in different days. An example of a stack of images is shown in fig. 2.4, on the vertical axis we may see different days, while on the horizontal axis we have the sub-apertures. Images on the same column are taken from the same position of the satellite in different days and images on the same row are taken in the same day but from different sub-apertures.

We will consider no temporal decorrelation, that means that the scene will not vary, so in consecutive days and in the same sub-aperture (same column of the Stack) the satellite will sense a constant ground reflectivity. This is an ideal case but changes in the scene can be considered like noise to be added to the thermal noise.

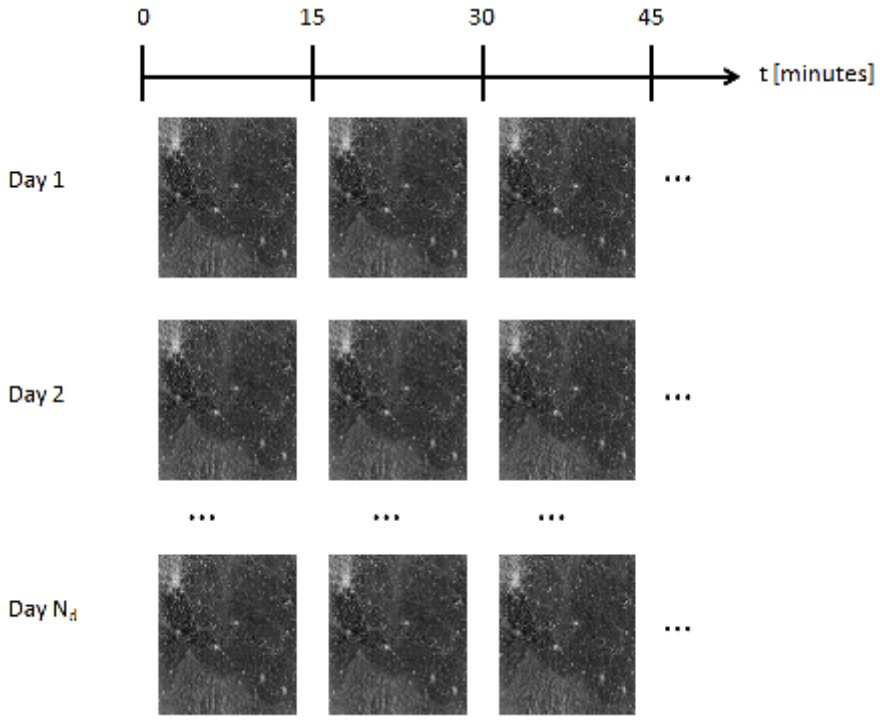

Figure 2.4: An example of a stack of images (images taken by Sentinel-1A [15])

Now that the concepts of atmospheric phase screen (along with its variogram and autocorrelation function) and stack have been defined, we should put them into formulas and write the model.

We will start from already focalized images.

If we call $a(x, y)$ the ground complex reflectivity, d_{APS} the atmospheric phase screen in millimeters, the received signal will be

$$y(x, y, s, d) = a(x, y, s)\, e^{j\frac{4\pi}{\lambda} d_{APS}(x,y,s,d)} + w(x, y, s, d) \tag{2.16}$$

where s indicates the sub-aperture, d the day the data were acquired and w the AWGN noise.

Since we will vectorize the data to process them and in order to simplify the formulas we can substitute the coordinate (x, y) with p, knowing that the number of pixels N_p in an image will be $N_x \times N_y$.

Furthermore, similarly to what we showed in equation 2.8 we can write

$$e^{j\frac{4\pi}{\lambda} d_{APS}(p,s,d)} = e^{j\phi_{APS}(p,s,d)} \tag{2.17}$$

From equation 2.17 we can notice that using a given frequency (or wavelength), there is a relation between the phase of the APS and the APS in mm.

The model can now be written in the following way:

$$y(p, s, d) = a(p, s)\, e^{j\phi_{APS}(p,s,d)} + w(p, s, d) \tag{2.18}$$

but as it was stated before we can not combine together images from different sub-apertures, therefore the dependence on s can be dropped, since only images from the same sub-aperture and consecutive days will be processed together. After we finished processing data from one sub-aperture we will move to the next one.

Exploiting this fact, the model can be simplified

$$y(p,d) = a(p)\, e^{j\phi_{APS}(p,d)} + w(p,d) \tag{2.19}$$

Equation 2.19 is the model we will start from in order to estimate the atmospheric phase screen.

As we said GEOSAR systems have been studied to work at frequencies between the L-Band and the the X-Band and the main differences are shown in fig. 2.1 and in table 2.1.

In order to estimate the atmosphere we are really interested in the phases of the different members of the model and in equation 2.8 it was shown the correspondence between phase of the APS and the APS in millimeters.

We have to check that at the two working frequencies the wrapping effect is not present. A situation in which the phase wraps around can create many problems because it would mean that there is an ambiguity in the phase-to-millimeter conversion. It might be really hard to understand the true phase in the presence of wrapping.

If we take a look at the simulation of an atmospheric phase screen with a power of 400 mm^2 (an average power) seen in L and X bands we can notice that only in one case there is no wrapping (fig. 2.5)

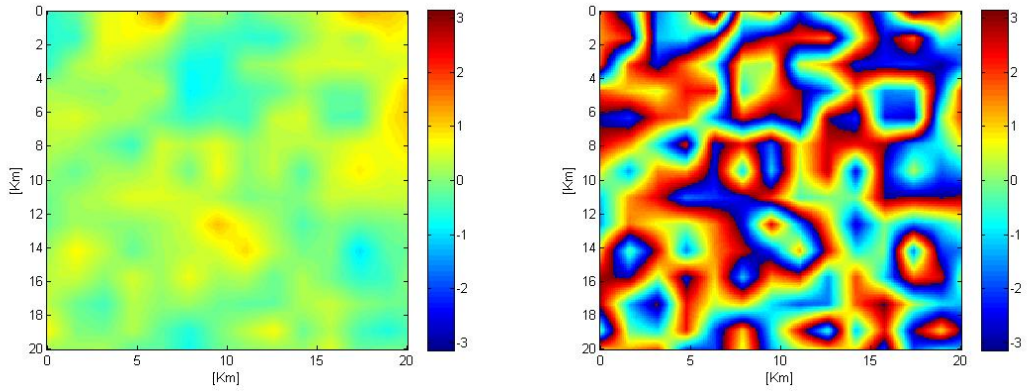

(a) L-band (b) X-band

Figure 2.5: APS seen in L and X bands, wrapping is present only in the X-Band

This fact can also be seen from equation 2.17, if we set the phase $\phi_{APS}(p, s, d)$ to 0 and 2π

$$\frac{4\pi}{\lambda} d_{APS} = 0 \qquad d_{APS} = 0$$

$$\frac{4\pi}{\lambda} d_{APS,wrap} = 2\pi \qquad d_{APS,wrap} = \frac{\lambda}{2}$$

With $\lambda = 0.3$ m (L-band) and $\lambda = 0.03$ m (X-band), the phase wrap around every 150 mm using the L-band and only 15 mm with the X-band. From this example it is clear that the best choice for estimating the APS is the L-band, since it is much more difficult to find the wrapping effect, even if we could achieve better range and azimuth resolution using the X-band (due to higher bandwidth and shorter wavelength).

In case we need higher resolution images we could perform SAR acquisitions in both L and X-band and use the L-band to estimate the atmospheric phase screen in millimeters, then we could convert it using equation 2.8 to what would be an APS sensed in the X-band and use it to remove the APS while focusing an X-band

image.

2.5 Phase model for APS estimation

In equation 2.19 the model has been shown, but in certain situations a simplified model can be used.

The model previously proposed is a non linear model and involves the use of complex numbers, but what we are most interested in is the phases of the targets in the scene and the phase of the APS.

If we take into account only the phases in the model we get

$$\arg\{y(p,d)\} = \phi(p,d) \qquad \arg\{a(p)\} = \phi_s(p)$$

where the s in $\phi_s(p)$ stands for scene, we obtain

$$\phi(p,d) = \phi_s(p) + \phi_{APS}(p,d) + tan^{-1}\left(\frac{\mathrm{Im}\left\{w(p,d)e^{-j(\phi_{APS}(p,d)+\phi_s(p))}\right\}}{|a(p)| + \mathrm{Re}\left\{w(p,d)e^{-j(\phi_{APS}(p,d)+\phi_s(p))}\right\}}\right) \tag{2.20}$$

in equation 2.20 the last term is the noise, if we call it $\tilde{\phi}_w(p,d)$, we get the simplified model:

$$\phi(p,d) = \phi_s(p) + \phi_{APS}(p,d) + \tilde{\phi}_w(p,d) \tag{2.21}$$

This model can be really useful because it is linear and uses only real numbers and this makes computations simpler.

It has a significant drawback though: we need to be careful that the phase does not wrap around otherwise we could get meaningless results, since a linear model can not take into account the wrapping effect.

2.6 Power budget

Hereafter we want to highlight the working conditions of the system.

If we want to see the performances of a GEOSAR system the parameters we are most interested in are the signal to noise ratio (SNR), range resolution and azimuth resolution.

We have already talked about resolution and shown the formulas that allow us to compute the azimuth and range resolutions.

How to compute the SNR is shown in Appendix B, here we will only write the final expression

$$SNR = P_M \left(\frac{G^2 \lambda^2 \eta_2}{(4\pi)^3 r_0^4} \right) \left(\sigma_{0,s} \frac{c}{2B \sin(\theta_I)} \frac{L_a}{2} \right) \left(\frac{T_S}{N_0} \right) \tag{2.22}$$

The first term is the average power, that is the product of the peak power and the duty cycle ($P_M = P_T d_c = P_T T_c f_{prf}$), the second term is the effect of the antenna gain (G), spherical divergency and total losses (η_2), the third term is the radar cross section of the targets (product of σ_0, ground resolution and azimuth resolution), the last term is the noise power in the extent of the matched filter, that is the duration of the synthetic aperture $T_S = \frac{\lambda r_0}{v L_a}$. We will be in a scenario shown in the following table.

Data	Symbol	Value	Unit
Peak power	P_T	2400	W
Antenna diameter	L_a	6	m
Antenna TX efficiency	η	-2.22	dB
Duty cycle	d_c	16	%
Frequency	f_0	1.27E+9	Hz
Bandwidth	B	2.2E+6	Hz
Noise Factor	F	3	dB
Slant range	r_0	3.74E+07	m
Satellite height	h_s	4.216E+07	m
Satellite velocity	v	5	m/s
Losses (rain and atmosphere)		3	dB
Mean reflectivity	σ_0	-15	dB
Integration Time	T	900	s
Range resolution	ρ_{rg}	85	m
Azimuth Resolution	ρ_{az}	1100	m
SNR		8.7	dB

Table 2.2: GEOSAR system parameters and working conditions

In the following chapters we will show few estimators to obtain the APS. Examples are shown with the SNR shown in table 2.2 (8.7 dB) that is the average SNR we expect (it may vary since it might experience different noise and losses). Moreover we will show the error versus the SNR, and we will set a limit under which we can consider the estimate to be good enough.

Chapter 3

APS estimation through MMSE estimator

The first method presented to estimate the atmospheric phase screen is by means of the Minimum Mean Square Error.
In this chapter we will use the simplified model (equation 2.21).

3.1 Ideal case: only APS

We will not consider the ground reflectivity for the moment, this is not a real case and will be used only for comparison with the case with the presence of the scene to see the performance loss.
The model is even simpler than the one in equation 2.21

$$\phi(p,d) = \phi_{APS}(p,d) + \tilde{\phi}_w(p,d) \tag{3.1}$$

where

$$\tilde{\phi}_w(p,d) = tan^{-1}\left(\frac{\mathrm{Im}\left\{w(p,d)e^{-j\phi_{APS}(p,d)}\right\}}{1+\mathrm{Re}\left\{w(p,d)e^{-j\phi_{APS}(p,d)}\right\}}\right) \tag{3.2}$$

and since taking into account just one image we have an equal number of unknowns (N_p) and data (N_p), also the dependence on d can be dropped.
Looking one image at a time

$$\phi(p) = \phi_{APS}(p) + \tilde{\phi}_w(p) \tag{3.3}$$

that with matrices is

$$\boldsymbol{\phi} = \boldsymbol{H}\boldsymbol{\phi}_{APS} + \tilde{\boldsymbol{\phi}}_w \tag{3.4}$$

Where $\mathbf{H}$ is an identity matrix ($N_p \times N_p$). From digital signal processing theory we know that for linear models with gaussian processes, the MMSE estimator is

$$\hat{\boldsymbol{\phi}}_{APS} = \boldsymbol{\mu}_{APS} + \boldsymbol{C}_{\phi_{APS}\phi_{APS}}\boldsymbol{H}^T \left(\boldsymbol{H}\boldsymbol{C}_{\phi_{APS}\phi_{APS}}\boldsymbol{H}^T + \boldsymbol{C}_{ww}\right)^{-1} \left(\boldsymbol{\phi} - \boldsymbol{H}\boldsymbol{\mu}_{APS}\right) \tag{3.5}$$

where $\boldsymbol{C}_{\phi_{APS}\phi_{APS}}$ and $\boldsymbol{C}_{ww}$ are the covariance matrices of $\boldsymbol{\phi}_{APS}$ and the noise respectively, $\boldsymbol{\mu}_{APS}$ is the expected value of the APS, but the atmospheric phase screen is a zero mean process and $\mathbf{H}$ is an identity matrix, so we can simplify the estimator

$$\hat{\boldsymbol{\phi}}_{APS} = \boldsymbol{C}_{\phi_{APS}\phi_{APS}} \left(\boldsymbol{C}_{\phi_{APS}\phi_{APS}} + \boldsymbol{C}_{ww}\right)^{-1} \boldsymbol{\phi} \tag{3.6}$$

We will assume to have a gaussian noise and to know its covariance ($\boldsymbol{C}_{ww}$).
The last equation shows the MMSE estimator for the phase of the APS, then we have to convert it to millimeters using equation 2.8.
An example of the estimate of the APS using this method is shown in fig. 3.1.
The Root Mean Square Error (RMSE) using this method is shown in fig. 3.2.
There is one last consideration to make: this estimator would be the best at

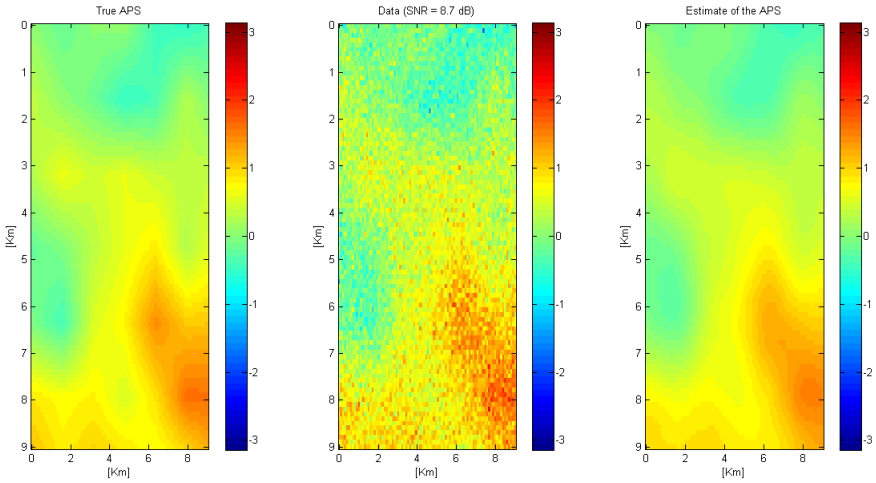

Figure 3.1: True APS seen in L-band (left); data with a SNR=8.7 dB (center); estimate of the phase of the APS (right)

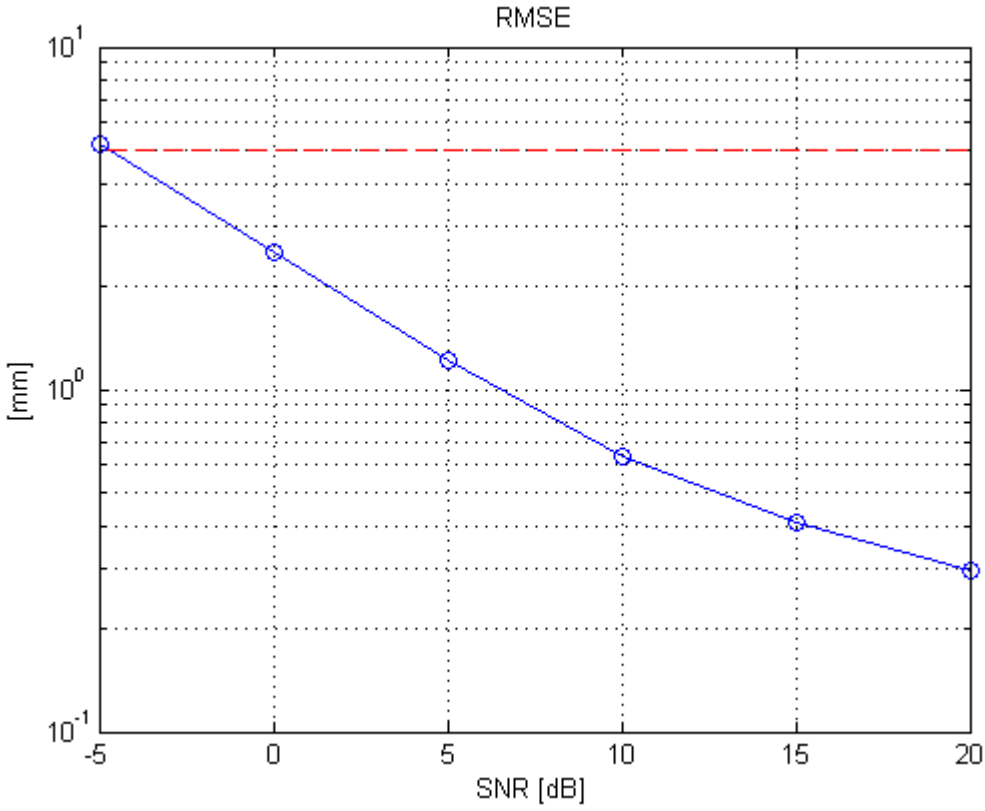

Figure 3.2: MMSE: RMSE without the scene (blue line), goal set at 5 millimiters (red dashed line)

minimizing the MSE, but in order to achieve this minimum error we should take into consideration every pixel of the image together and the covariance of the phase should take into account the correlation of each target. This would mean a huge covariance matrix ($N_p \times N_p$), the problem is not only the big matrix, but the fact that we have to compute the inversion of such a matrix and this procedure is going to require a lot of time.

A wise method to improve the speed of this estimator is to split the images in smaller sections and use the estimator in 3.6 on these regions and then combine the sections to recreate the whole image.

Due to the fact that we use only close points to estimate the APS and their correlations, and we do not take into account informations from farther points there is going to be a small performance loss (slightly bigger error).

Fig. 3.3 shows the RMSE if we split the image into 25 smaller images, the error is almost the same, but the estimator is much faster (about 400 times faster).

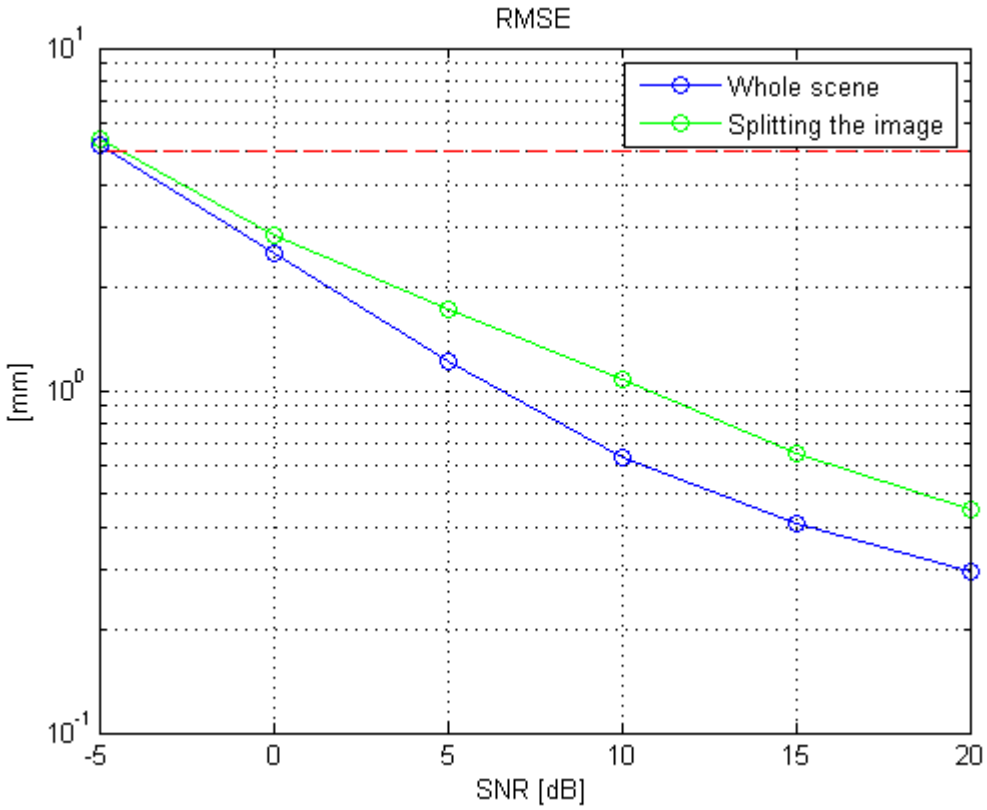

Figure 3.3: MMSE: Comparison between the error in case we consider the whole image (blue line) and in case we split the image into 25 smaller images (green line), goal set at 5 millimiters (red dashed line)

3.2 Average and MMSE estimator

Now we add the ground reflectivity (with no temporal decorrelation) and use the model in equation 2.21.

In this model we have more unknowns ($N_p + N_p \times N_d$) than data ($N_p \times N_d$) we have to find a way to reduce the number of unknowns.

One possible method to reduce the number of unknowns is to exploit the fact that the scene remains unchanged in consecutive days, if looked from the same sub-aperture.

If we consider the model in equation 2.19, we can notice that every process is zero mean, but while the ground reflectivity remains the same in consecutive days, the

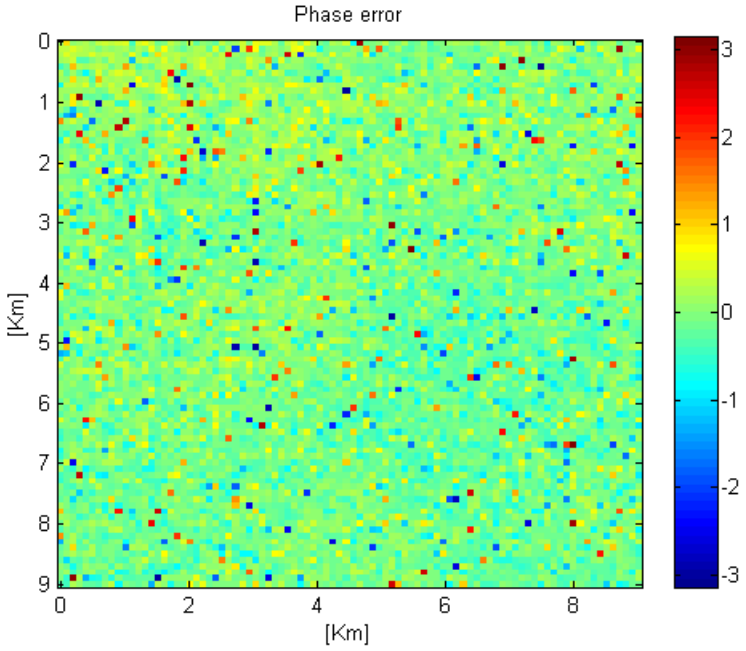

Figure 3.4: Phase error of the estimate of the ground reflectivity through average over 10 days (SNR=8.7)

atmospheric phase screen and the noise vary.

If we average the images of the same sub-aperture in N_d consecutive days, we will notice that we are adding N_d times the same scene and the APS and noise will tend to cancel out, leaving us only the scene.

In this way we get an estimate of the ground reflectivity

$$\hat{a}(p) = \frac{1}{N_d} \sum_{d=1}^{N_d} y(p, d) \tag{3.7}$$

This is a good estimate of the ground reflectivity, an example of the estimate of the phase of the scene is shown is fig. 3.4.

The error in the estimate of the phase of the scene can be considered a noise to be added to the thermal noise.

Now we can remove the phase of the scene from the model in equation 2.19 multiplying everything by the complex conjugate of the scene just estimated.

$$\tilde{y}(p,d) = y(p,d) \circ \hat{a}^*(p) \tag{3.8}$$

where $\circ$ indicates the Hadamard product, so we get

$$\tilde{y}(p,d) = a(p)e^{j\phi_{APS}(p,d)} \circ \hat{a}^*(p) + w(p,d) \circ \hat{a}^*(p) \tag{3.9}$$

Looking at the phases of the components of the last equation we get

$$\tilde{\phi}(p,d) = \phi_{APS}(p,d) + \tilde{\phi}_w(p,d) \tag{3.10}$$

The model we obtained is really similar to the one in equation 3.3.
The phase noise will be stronger than the previous one because it will contain the previous phase noise plus the phase error of the estimate of $a(p)$.
Now we can replicate the steps applied in the ideal case without the ground reflectivity and looking at one image at a time we can use a MMSE estimator on the model in equation 3.10.
The error will be bigger than the one without scene due to the fact that in the previous case we can think that we knew the phase of the scene and removed it; now we have to estimate it through an average with zero mean processes, but we will get an error in estimating the ground reflectivity that will affect the MMSE estimator.
The error in the estimate of the scene will be due to two factors that we have to consider:

- we should average over many days (ideally infinite) to get an average of the atmospheric phase screen and the noise that is equal to zero,
- if we use many days to compute the average we would get an almost zero mean APS and noise but with higher variance, and over many days the scene

will change.

This shows that there is a trade-off in chosing the number of days to be use in the average estimator.

We should also consider that it might be true that there is a small temporal decorrelation in consecutive days, but that may not be the case if we take into account too many days.

Fig. 3.5 and fig. 3.6 present an example of this estimator (estimate of the APS and RMSE respectively).

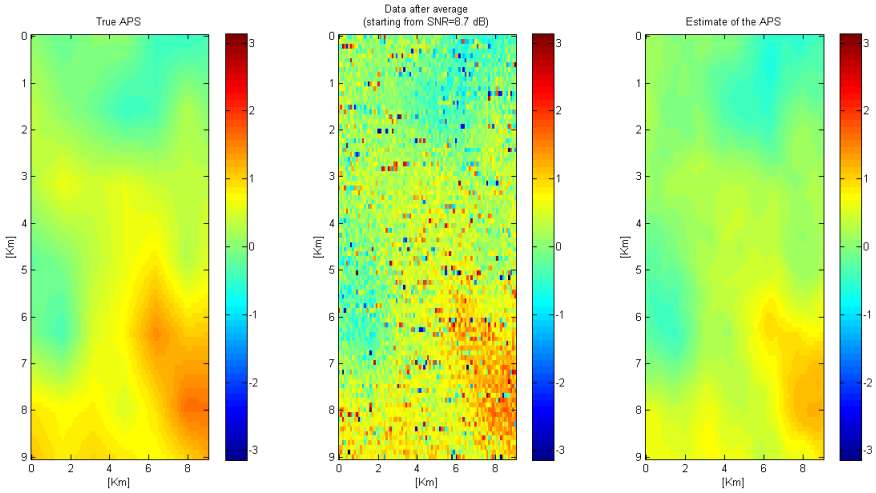

Figure 3.5: MMSE: Estimate of the APS with average estimator (right), true APS (left), data after removal of the scene through average with SNR=8.7 dB (middle)

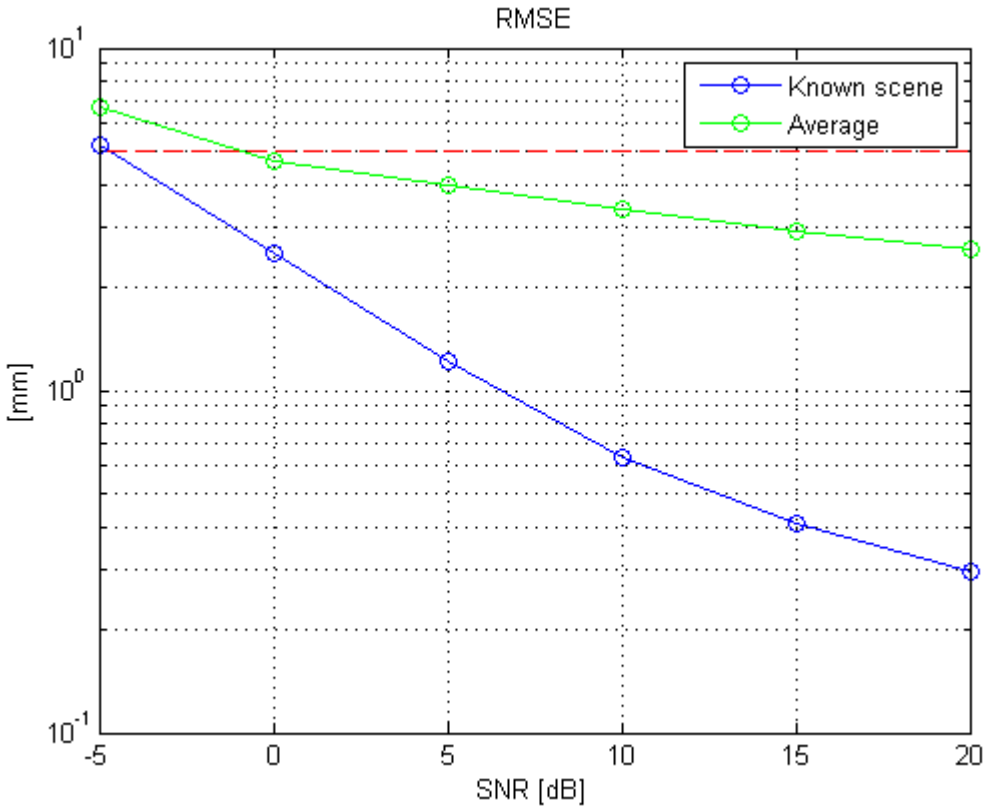

Figure 3.6: MMSE: RMSE with average and MMSE estimator (green line) and a comparison with the ideal case (blue line), goal set at 5 millimiters (red dashed line)

The RMSE in fig. 3.6 has been obtained using the whole data together (and thus a really big covariance matrix to be inverted was involved), as we said in the case with known scene we can speed up the estimator dividing the images in smaller areas; there will be a small performace loss shown in fig. 3.7, where the image has been divided in 25 smaller areas.

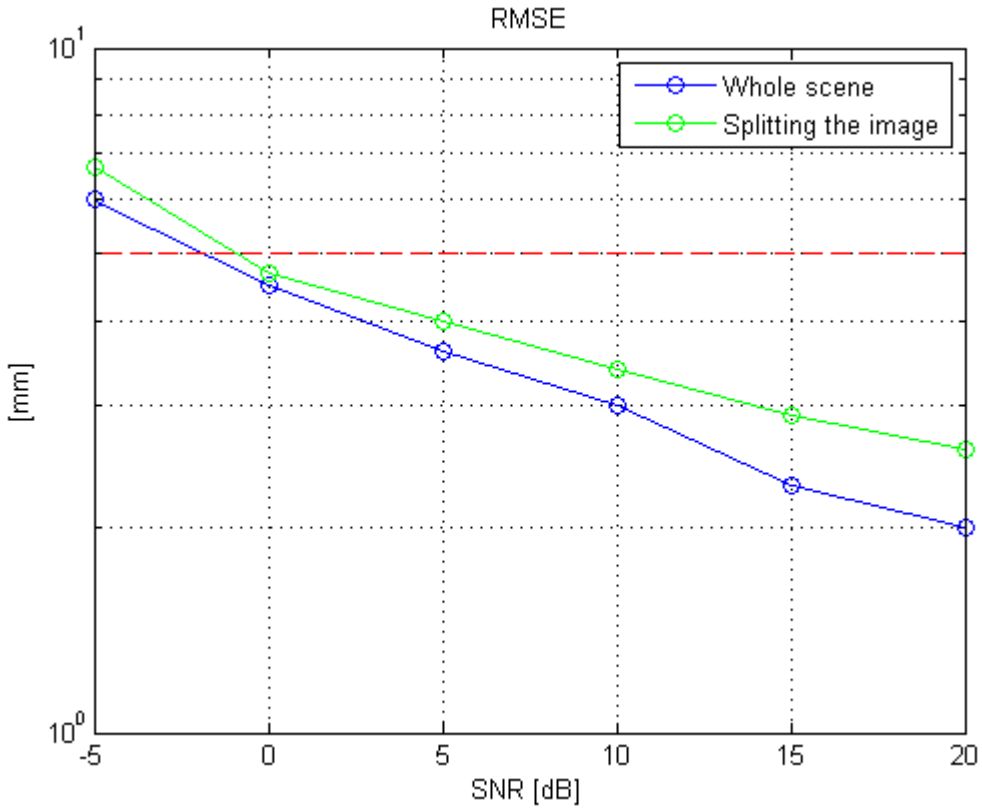

Figure 3.7: MMSE: RMSE with average estimator and use of smaller ares (green line) and a comparison with the estimator using the whole scene (blue line), goal set at 5 millimiters (red dashed line)

Chapter 4

APS estimation through SVD

In this chapter we will present a method that exploits the fact that the model shown in equation 2.19 is actually a separable model that we can see in the following way (the idea of looking it as a separable model was taken from [16], where the SVD was used to look for permanent scatterers)

$$y = u \cdot v + w \tag{4.1}$$

Where u contains information on the ground reflectivity and v contains information on the APS.

We can try to separate this model by means of a Singular Value Decomposition (SVD), but we need to take into account informations from more than one day.

We can rewrite the model in matrix form

$$\boldsymbol{Y} = \boldsymbol{U}\boldsymbol{\Lambda}\boldsymbol{V} + \boldsymbol{W} \tag{4.2}$$

In this case $\boldsymbol{U}$ and $\boldsymbol{V}$ are matrices that contain information on the scene and the APS in different days respectively.

Matrix $\boldsymbol{\Lambda}$ contains the singular values of the SVD, but we will not look at this matrix since it does not contain meaningful information for estimating the atmo-

spheric phase screen.

Matrix $\boldsymbol{Y}$ is the data from the images acquired with the SAR acquisitions. Once again we have to take into account few days in order to have more data than unknowns.

Furthermore we have to split the images into smaller sections of dimensions $\tilde{N}_p \times \tilde{N}_p$ (with $\tilde{N}_p \ll N_p$) for two main reason:

- if we use smaller areas, the time required for the computation of the SVD would decrease,
- the SVD will assign the same value for the atmosphere to each pixel in the same area, so if we use the whole image we would obtain an almost flat atmospheric phase screen. In fig. 4.1 this effect is shown selecting a high SNR.

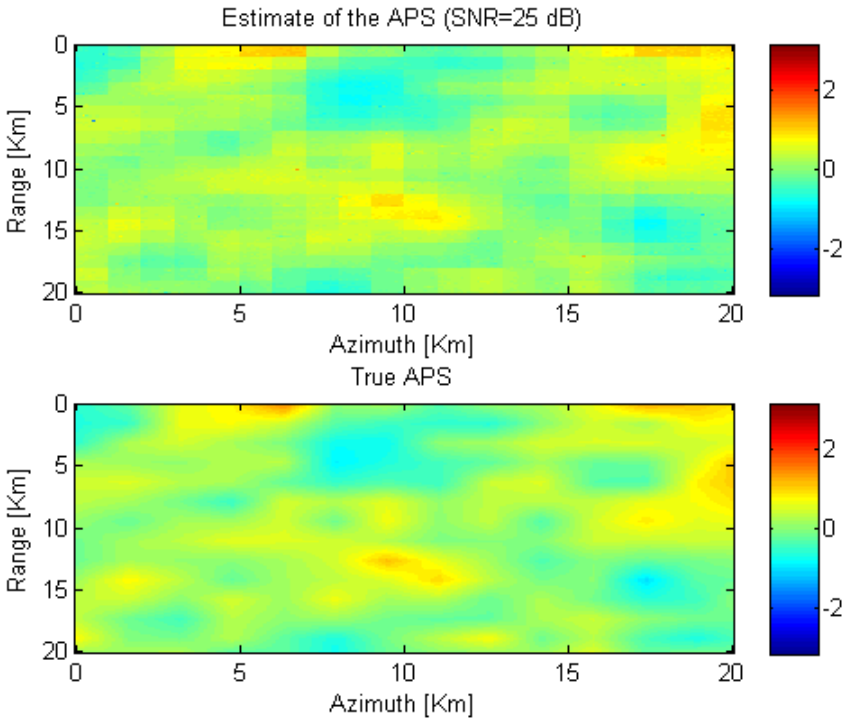

Figure 4.1: The SVD tends to assign the same value to the APS in the area where it is computed, so in the estimate we will see the images divided in big squares (figure above).

We still have to be careful not to choose sections that are too small, otherwise the noise would affect too much the SVD.

As we said, matrix $\boldsymbol{Y}$ will contain the data from the same areas of the images taken in consecutive days and it has to have the following structure

$$\boldsymbol{Y} = \begin{bmatrix} y(1,1) & y(1,2) & \cdots & y(1,N_d) \\ y(2,1) & y(2,2) & \cdots & y(2,N_d) \\ \vdots & \vdots & \ddots & \vdots \\ y(\tilde{N}_p,1) & y(\tilde{N}_p,2) & \cdots & y(\tilde{N}_p,N_d) \end{bmatrix}$$

This matrix $\boldsymbol{Y}$ will be the input of the SVD.

The SVD will return three matrices $\boldsymbol{U}, \boldsymbol{\Lambda}, \boldsymbol{V}$

$$[\boldsymbol{U}, \boldsymbol{\Lambda}, \boldsymbol{V}] = svd\,(\boldsymbol{Y}) \tag{4.3}$$

Matrices on the left side of the equal sign will have the following dimensions:

- $\boldsymbol{U}$: $\tilde{N_p}^2 \times \tilde{N_p}^2$
- $\boldsymbol{\Lambda}$: $\tilde{N_p}^2 \times N_d$
- $\boldsymbol{V}$: $N_d \times N_d$

The first column of $\boldsymbol{U}$ contains the informations on the ground reflectivity, we can reconstruct an image of $N_p \times N_p$ pixels using this column, while the other columns can be discarded.

The first column of $\boldsymbol{V}$ contains the informations on the phase of the atmospheric phase screen. It consists of N_d values that have to be assigned to the areas of the N_d days used to compute the SVD. The value in $V(1,1)$ has to be assigned to the whole area of the first day, $V(2,1)$ to the area of the second day and so on. The

other columns can be discarded.
As stated before $\mathbf{\Lambda}$ can be ignored.

There is still one more relevant issue to be discussed, the SVD will find more than one solution to our problem, because given a possible solution, another one can be found simply rotating every obtained value by a constant phase. This would still yield a good result.
The SVD does not know which one is the true solution, thus it will add a constant phase to every term so that $V(1,1)$ has a phase that is equal to zero (the SVD sets $V(1,1)$ to a real number).
It is up to us to solve the problem of the constant phase term, but we need additional informations.
Hereafter we will present a few method to estimate this phase constant starting from a scenario with a strong assumption and then moving on to more realistic cases.

4.1 Ideal case: known scene

In order to solve the problem of the phase constant introduced by the SVD we will start from the same assumption we made in the previous chapter with the MMSE estimator.
We will assume to know exactly the ground reflectivity for the moment.
The scene is still $a(p)$ and it is completely known, if we call $\tilde{a}(p)$ the first estimate of the ground reflectivity taken from the first column of $\boldsymbol{U}$, we should have that $\tilde{a}(p)$ is $a(p)$ rotated by the constant phase term

$$\tilde{a}(p) = a(p)e^{j\phi_{const}} \tag{4.4}$$

if we multiply $\tilde{a}(p)$ by the complex conjugate of $a(p)$, looking at the phase of the result we should find out the phase constant term

$$\hat{\phi}_{const} = \arg\{\tilde{a}(p)a^*(p)\} = \arg\left\{|\tilde{a}(p)|\,|a(p)|\,e^{j(\phi_a+\phi_{const}-\phi_a)}\right\} \tag{4.5}$$

ϕ_{const} is a constant for every pixel in the area for every day, therefore we could use only one target to estimate the ϕ_{const}, but there is also noise to be taken into account, so if we just pick a point randomly, it could be affected too much by noise and that might ruin the estimate of that given area. A better choice would be to compute it for every point (so the error would not be affected too much if we pick a noisy point)

$$\hat{\boldsymbol{\phi}}_{const} = arg\{\tilde{\boldsymbol{a}} \circ \boldsymbol{a}^*\} \tag{4.6}$$

where $\circ$ is the Hadamard product.

This $\hat{\boldsymbol{\phi}}_{const}$ is actually a correction that has to be applied to the phase of the APS estimated with the first column of $\boldsymbol{V}$

$$\hat{\phi}_{APS}(p,d) = \arg\left\{e^{j\arg\{V(d,1)\}}e^{-j\hat{\phi}_{const}(p,d)}\right\} \tag{4.7}$$

Using this method we can get estimates of the APS that look like the image shown in fig. 4.2

From the estimate shown in fig. 4.2 we may see that noise has a big impact on the performance of the SVD estimator. Looking at the Root Mean Square Error (RMSE) shown in fig. 4.3 we can notice that the error is too high, the estimate is not good enough.

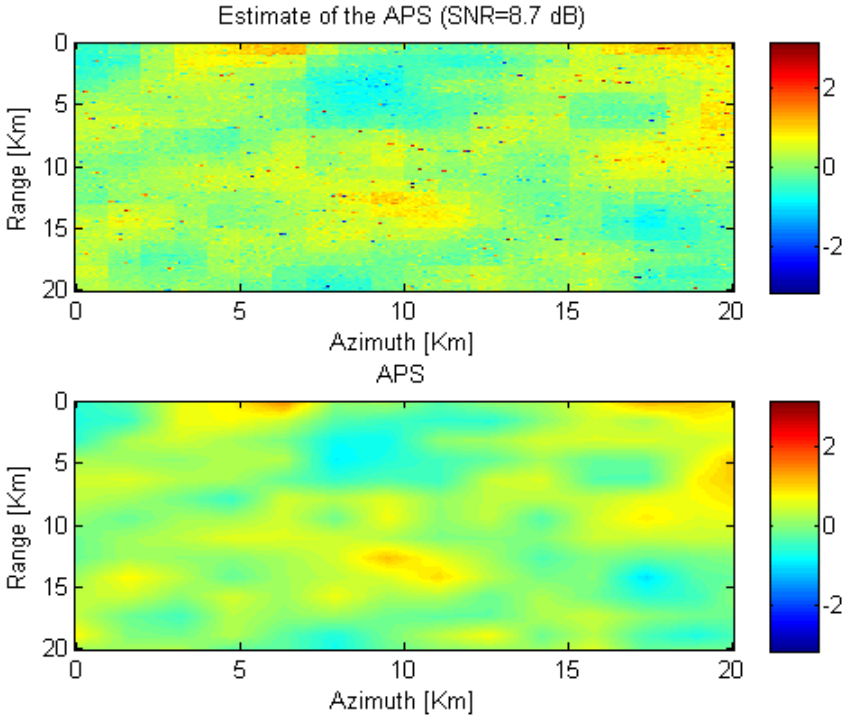

Figure 4.2: Estimate of the APS (above) achieved by means of the SVD with a SNR=8.7 dB; true APS (below).

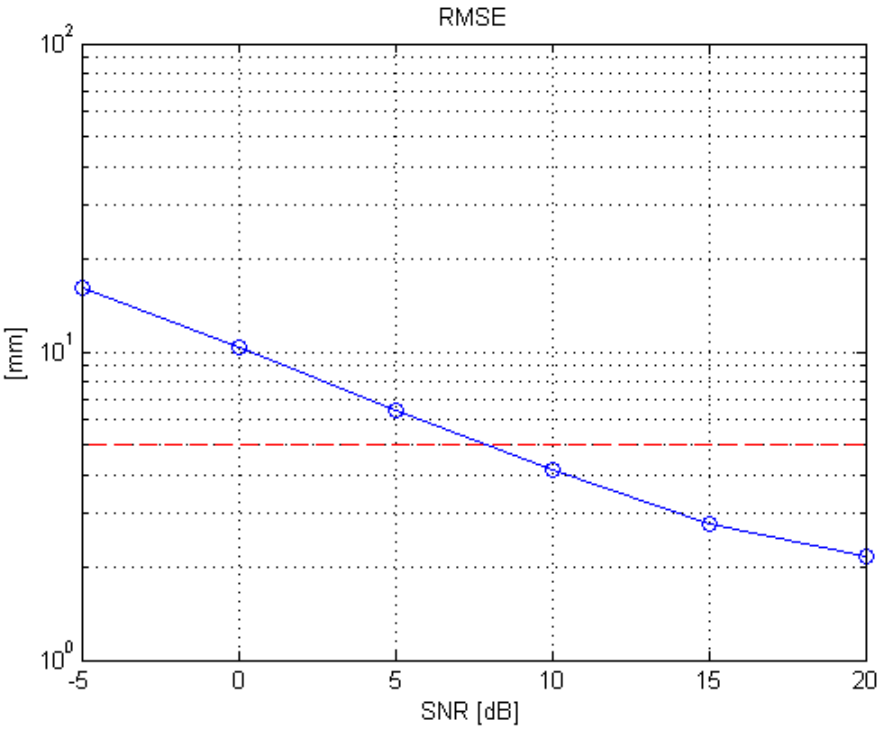

Figure 4.3: RMSE with known scene, the error is high due to the noise in the estimate (like in fig. 4.2, goal set at 5 millimiters (red dashed line)

4.1.1 Improvement in the estimate using multi-look

A common method to decrease the impact of the noise on the estimate is the use of the multi-look in range, it consists on a sliding window that is used to average the values along the range direction.

We can slightly improve the estimate of the atmospheric phase screen using the multi-look in range, but we can still do better, reminding that the SVD assigns the same value to the area over which we compute it, we may notice that the differences are only due to the noise. If we average every pixel in the area we should be able to cancel the noise.

Using this method we should get an estimate of the APS that has flat areas, and steps between them, as shown in fig. 4.4.

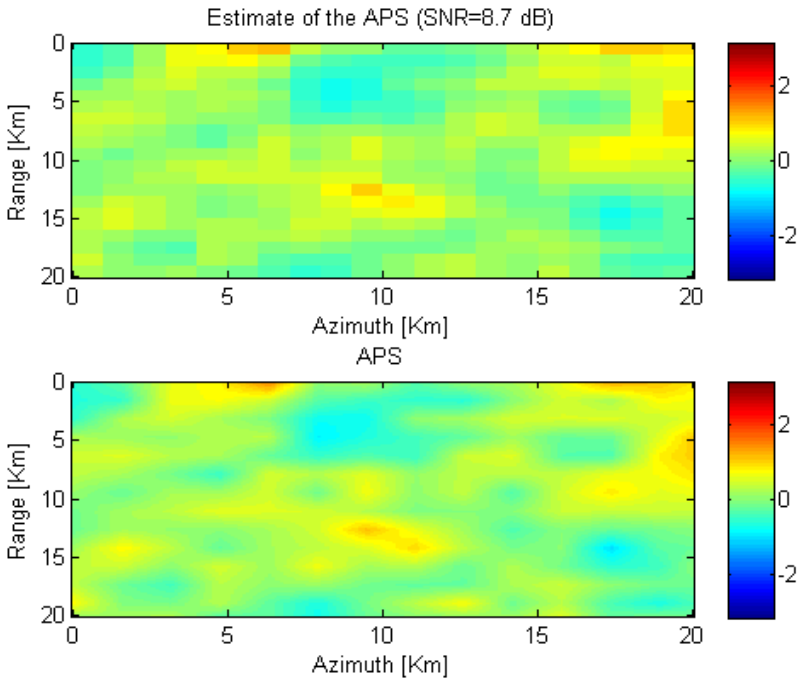

Figure 4.4: Estimate of the APS averaging over the area used to compute the SVD with a SNR=8.7 dB (above); true APS (below).

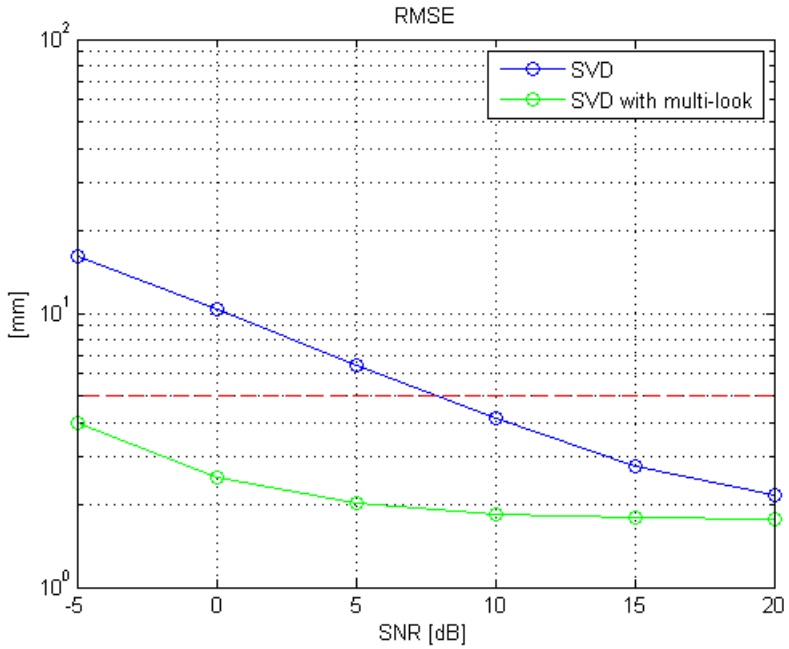

Figure 4.5: Comparison of the RMSE in the cases shown, plain SVD (blue line), averaging over the area (green line), goal set at 5 millimiters (red dashed line).

The estimate of the APS improves, so the RMSE decreases: fig. 4.5.

4.2 One Permanent Scatterer per area

We now remove the assumption to perfectly know the scene, and we assume that we only know one coefficient of the ground reflectivity per area in which we will compute the SVD.

This assumption is not so unreasonable since we might find some permanent scatterers in the scene. These targets are points that present a constant ground reflectivity.

We have to search for these targets looking at which pixels remain unchanged in the scene observing them for many days. Among these targets we can select the ones with greater amplitude, so that they would be more resistent to the thermal noise.

The steps to obtain the estimate of the APS have already been shown, we would

start by computing the SVD in equation 4.3, then from the first column of $\boldsymbol{U}$ we have to reconstruct the scene ($\tilde{a}(p)$) rotated by the phase constant, and finally we can estimate the phase constant similarly to what we did in equation 4.5

$$\hat{\phi}_{const} = \arg\left\{\tilde{a}(\bar{p})a^*(\bar{p})\right\} \tag{4.8}$$

where $\bar{p}$ indicates the permanent scatterer.

Then we have to remove this phase constant from the phase of the estimate of the APS

$$\hat{\phi}_{APS}(p,d) = \arg\left\{e^{j\arg\{V(d,1)\}}e^{-j\hat{\phi}_{const}}\right\} \tag{4.9}$$

Using this estimator, we may get an APS estimate as shown in figure 4.6 and a RMSE like in figure 4.7.

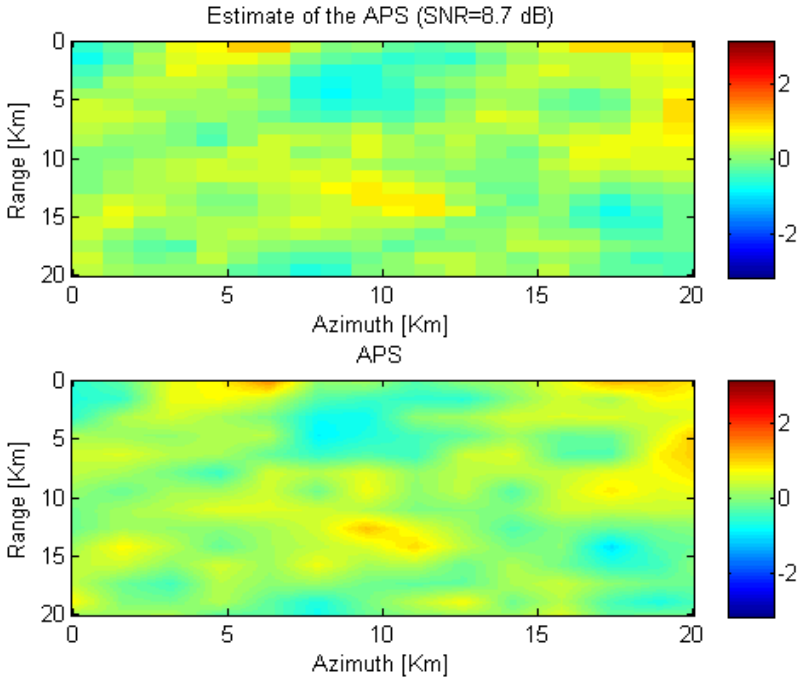

Figure 4.6: APS estimate (above) knowing 1 permanent scatterer per area (SNR=8.7 dB); true APS (below).

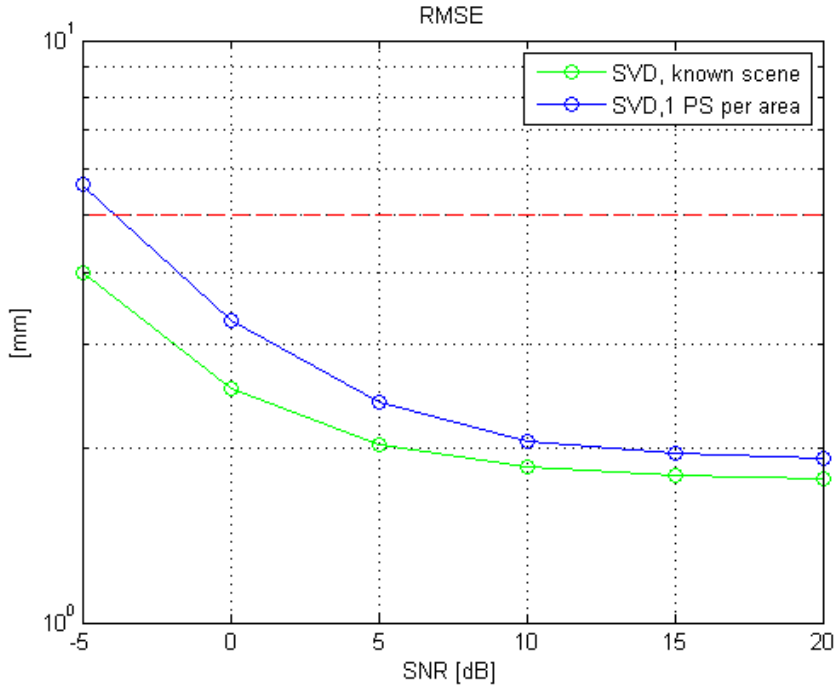

Figure 4.7: Root mean square error of the estimate of the APS knowing only 1 permanent scatterer per area (blue line); RMSE with known scene (green line) like in fig. 4.5, goal set at 5 millimeters (red dashed line).

4.3 Only one Permanent scatterer in the whole scene known

Now we will move on to more stringent assumption, we will assume to know only one ground reflectivity coefficient in the whole scene.

Knowing only one permanent scatterer, we can estimate only one phase constant to be corrected in the area where the permanent scatterer is situated. This will be done using equations 4.8 and 4.9.

Processing data from other areas in the way we did before is useless, we can not distinghuish the ground reflectivity and the atmospheric phase screen (we need a way to estimate the phase constant). We need to slighly overlap the areas, so that starting from areas adjacent to the one we are able to estimate, we can say

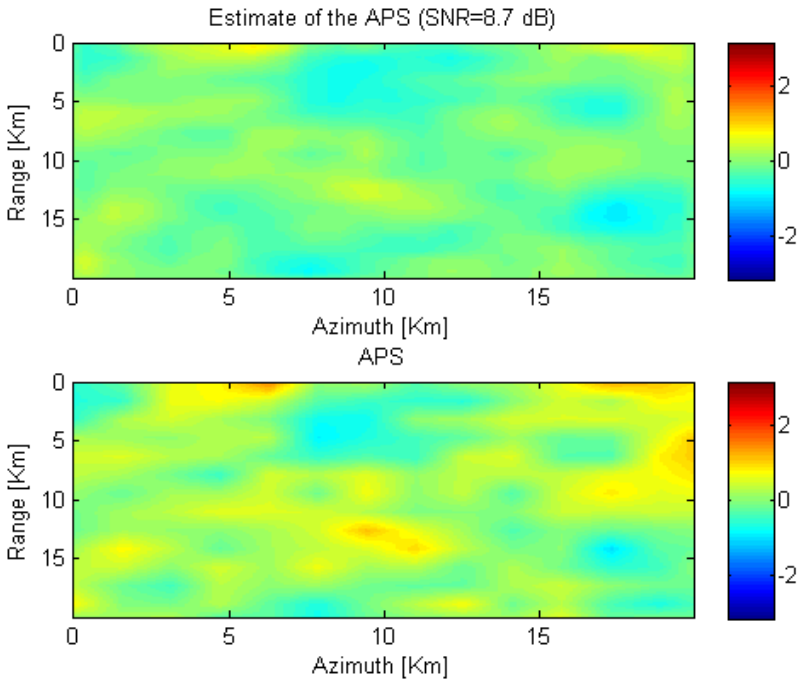

Figure 4.8: Estimate of the APS knowing only 1 target's reflecivity and exploiting overlapping areas with SNR=8.7 dB (above); true APS (below)

that the targets in the overlapped section must have the same values of APS and ground scene. In this way we should be able to estimate the phase constant of areas adjacent to the one with the permanent scatterer. Overlapping every area we should be able to estimate the phase constant and remove it from the whole image. Fig. 4.8 and fig. 4.9 show an example of the estimate of the APS and the RMSE respectively using this method.

We may notice that the RMSE increases a lot compared with the prevoius case, this is due to the fact that the SVD tends to assign a constant value to the APS of an area and saying that the overlapping targets have the same APS tends to assign to adjacent areas similar values.

This fact tends to squeeze the high and low values to values closer to zero, as we can see in fig. 4.8.

Although the RMSE is high in this case, we can find more than one permanent scatterer in the scene to estimate the phase constant and use the overlap only in

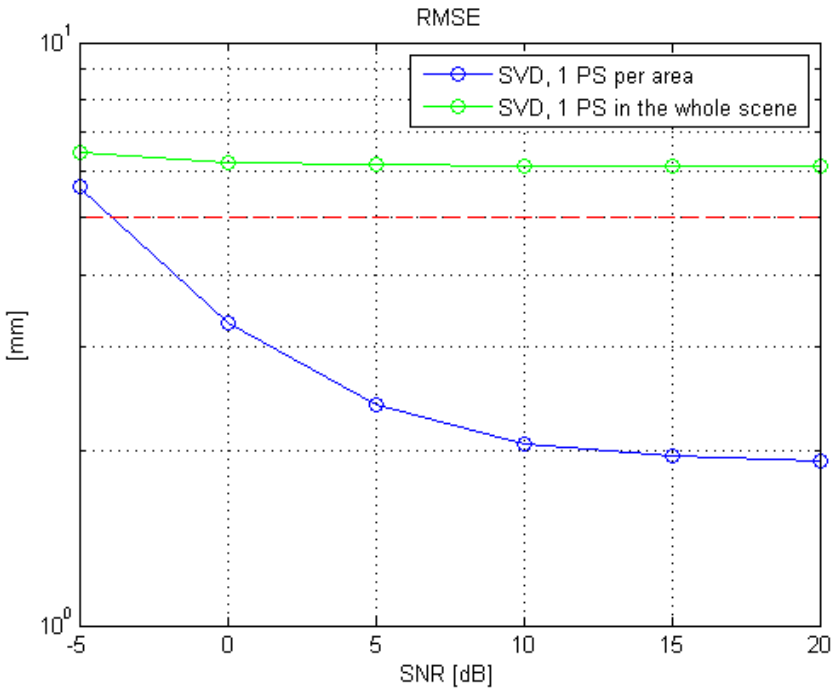

Figure 4.9: RMSE of the estimate of the APS knowing only 1 target's reflecivity and exploiting overlapping areas (green line); knowing 1 PS per area (blue line), goal set at 5 millimeters (red dashed line)

areas where there are no PS to estimate the phase constant there.

With some permanent scatterers and some areas estimated through overlapping, the RMSE will decrease and will get closer to the blue line in fig 4.9.

Chapter 5

APS estimation through ML estimator

In this chapter we will present the last algorithm to estimate the atmospheric phase screen, we will start from the model in equation 2.19 and we will implement a Maximum Likelihood Estimator (MLE).

We can write the model as

$$y(p,d) = a(p)e^{j\frac{4\pi}{\lambda}d_{APS}(p,d)} + w(p,d) = \hat{y}(p,d) + w(p,d) \tag{5.1}$$

The maximum likelihood estimator is the one that finds the maximum of the probability density function $f(\boldsymbol{y}|\boldsymbol{a},\boldsymbol{\phi}_{APS})$, it basically finds the most probable $\hat{y}(p,d)$ that fits the data and that will be our estimate.

Since the noise is a gaussian process the pdf will be gaussian and it will be

$$f(\boldsymbol{y}|\boldsymbol{a},\boldsymbol{\phi}_{APS}) = \frac{1}{\sqrt{(2\pi)^{N_pN_d}\left|\boldsymbol{C}_w\right|}} exp\left(-\frac{1}{2}\left(\boldsymbol{y}-\hat{\boldsymbol{y}}(\boldsymbol{a},\boldsymbol{\phi}_{APS})\right)^H \boldsymbol{C}_w^{-1}\left(\boldsymbol{y}-\hat{\boldsymbol{y}}(\boldsymbol{a},\boldsymbol{\phi}_{APS})\right)\right) \tag{5.2}$$

Now we have to find the values of $a(p)$ and $\phi_{APS}(p,d)$ that maximaze the previous pdf

$$\boldsymbol{a}, \boldsymbol{\phi}_{APS} = \arg \max_{\boldsymbol{a}, \boldsymbol{\phi}_{APS}} \{f(\boldsymbol{y}|\boldsymbol{a}, \boldsymbol{\phi}_{APS})\} \tag{5.3}$$

A common and useful method to solve equation 5.3 is to use the log form of the pdf, that means to compute the natural logarithm of of both side of the equation. What we get is

$$\begin{aligned} \ln\left[f(\boldsymbol{y}|\boldsymbol{a}, \boldsymbol{\phi}_{APS})\right] &= -\frac{N_p N_d}{2}\ln(2\pi) - \frac{1}{2}\ln\left(|\boldsymbol{C}_w|\right) + \\ &\quad -\frac{1}{2}\left(\boldsymbol{y} - \hat{\boldsymbol{y}}(\boldsymbol{a}, \boldsymbol{\phi}_{APS})\right)^H \boldsymbol{C}_w^{-1}\left(\boldsymbol{y} - \hat{\boldsymbol{y}}(\boldsymbol{a}, \boldsymbol{\phi}_{APS})\right) \end{aligned} \tag{5.4}$$

Looking at the left side of the equal sign we can distinguish three terms, computing the maximum of the pdf we can neglect the first and the second terms since they are constant. Looking at the third term we can neglect the $\frac{1}{2}$ constant and since there is a minus sign we can look for the minimum

$$\boldsymbol{a}, \boldsymbol{\phi}_{APS} = \arg \min_{\boldsymbol{a}, \boldsymbol{\phi}_{APS}} \left\{\left(\boldsymbol{y} - \hat{\boldsymbol{y}}(\boldsymbol{a}, \boldsymbol{\phi}_{APS})\right)^H \boldsymbol{C}_w^{-1}\left(\boldsymbol{y} - \hat{\boldsymbol{y}}(\boldsymbol{a}, \boldsymbol{\phi}_{APS})\right)\right\} \tag{5.5}$$

If we call the argument to be minimized $g(\boldsymbol{a}, \boldsymbol{\phi}_{APS})$ we can write

$$g(\boldsymbol{a}, \boldsymbol{\phi}_{APS}) = \left(\boldsymbol{y} - \hat{\boldsymbol{y}}(\boldsymbol{a}, \boldsymbol{\phi}_{APS})\right)^H \boldsymbol{C}_w^{-1}\left(\boldsymbol{y} - \hat{\boldsymbol{y}}(\boldsymbol{a}, \boldsymbol{\phi}_{APS})\right) \tag{5.6}$$

Now we have to minimize $g(\boldsymbol{a}, \boldsymbol{\phi}_{APS})$, so we have to compute the derivatives w.r.t $a(p)$ and $d_{APS}(p, d)$ and set them to zero

$$\begin{cases} \dfrac{\partial}{\partial a^*(p)} g(\boldsymbol{a}, \boldsymbol{\phi}_{APS}) = 0 \\ \dfrac{\partial}{\partial d_{APS}(p, d)} g(\boldsymbol{a}, \boldsymbol{\phi}_{APS}) = 0 \end{cases} \tag{5.7}$$

The derivative w.r.t $a(p)$ is really simple but the second derivative requires some steps, the computation is quite long and it is shown in Appendix C; the results will be

$$\begin{cases} \hat{a}(p) = \frac{1}{N_d} \sum_{d=1}^{N_d} y(p,d) e^{-j\frac{4\pi}{\lambda} d_{APS}(p,d)} \\ \hat{\phi}_{APS}(p,d) = tan^{-1}\left(\frac{\sum_{\tilde{p}=1}^{\tilde{N}_p} [\mathrm{Re}\{a(\tilde{p})\}\mathrm{Im}\{y(\tilde{p},d)\} - \mathrm{Im}\{a(\tilde{p})\}\mathrm{Re}\{y(\tilde{p},d)\}]}{\sum_{\tilde{p}=1}^{\tilde{N}_p} [\mathrm{Re}\{a(\tilde{p})\}\mathrm{Re}\{y(\tilde{p},d)\} - \mathrm{Im}\{a(\tilde{p})\}\mathrm{Im}\{y(\tilde{p},d)\}]} \right) \end{cases} \tag{5.8}$$

Where $\tilde{p}$ is a point in a space interval ($\tilde{N}_p$) where the APS can be considered constant, this is an approximation to make the computation simpler.

If we look carefully at the MLE in the system 5.8 we might notice that we actually need $\hat{a}(p)$ from the first equation to solve the second equation, and we need $\hat{\phi}_{APS}(p,d)$ from the second to solve the first one.

A simple method to solve the system is to solve it iteratively.

Looking at the first equation we can see that the estimate $\hat{a}(p)$ is obtained by averaging the data after removing the APS; at the first iteration, if we consider $d_{APS} = 0$ we obtain $\hat{a}(p)$ as the average of the data (exactly like in the MMSE chapter in equation 3.7).

Then we can use $\hat{a}(p)$ in the second equation to estimate the APS.

After we get a first estimate of $\phi_{APS}(p,d)$, we can start the second iteration inserting the APS into the first equation and that should yield a better estimate $\hat{a}(p)$ that can improve the estimation of $\phi_{APS}(p,d)$. We can go on with more iteration.

Fig. 5.1 and fig. 5.2 show an example of estimate of the atmospheric phase screen and how the RMSE varies with the iterations.

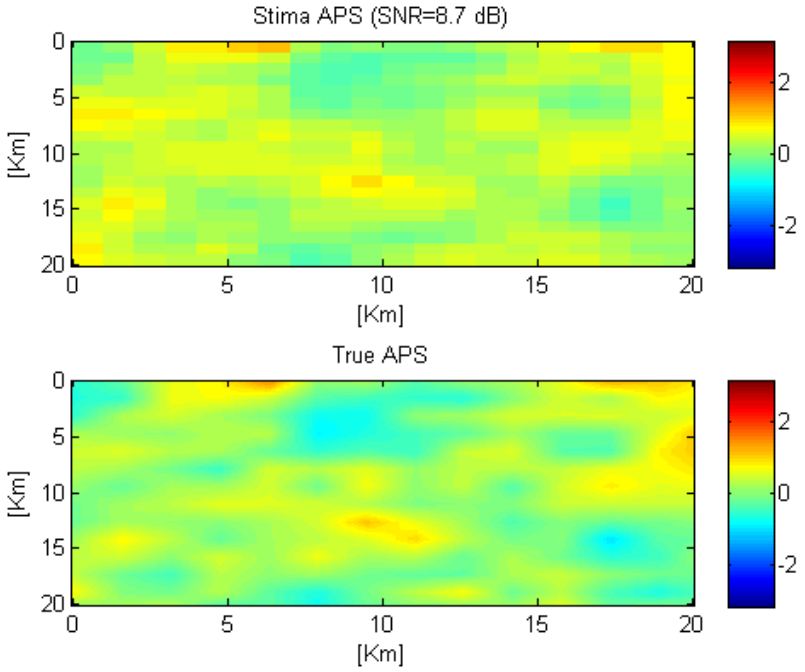

Figure 5.1: MLE: Estimate of the APS (above) with a SNR=8.7 dB, true APS (below)

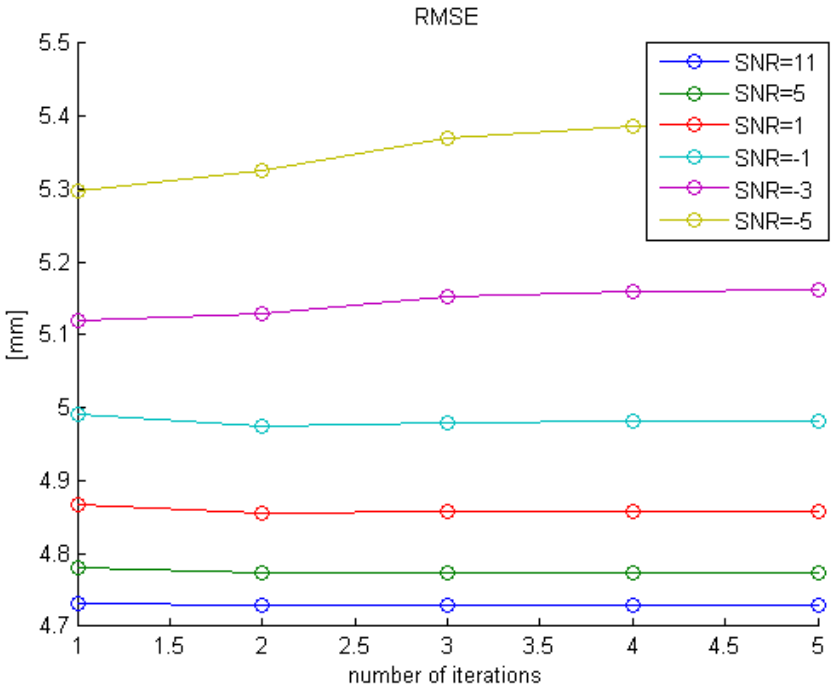

Figure 5.2: MLE: RMSE vs iterations

It can be noticed that we are not estimating the atmospheric phase screen in a good way since the RMSE actually worsens with more iterations (or at best remains constant). This is due to the fact that we are estimating the APS dividing it in areas that we assume to have constant values.
A possible solution would be to decrease the size of the area where we consider the APS to be constant, this would yield an image with better resolution of the APS, but if we decrease the size too much the noise might impact to much the estimator and we would still have areas where the APS would have the same values.
A better solution would be the following, before moving to a new iteration, we can smooth the edges between adjacent areas of the atmospheric phase screen filtering the image with a square window about the size of the areas.
This improve the estimate of the APS and thus the estimate in the following iteration.
We can notice this by looking at fig. 5.3 and fig. 5.4 that show an example of estimate of the atmospheric phase screen and how the RMSE varies with the iterations applying this spatial filter.

From fig. 5.4 we may notice that there is an improvement in the estimate of the atmospheric phase screen at the second iteration, but after that the error remains almost constant, so it does not make sense to make many iterations, two are enough.
Fig. 5.5 shows the RMSE of the estimate of the atmospheric phase screen after the second iteration when we apply the spatial filter.

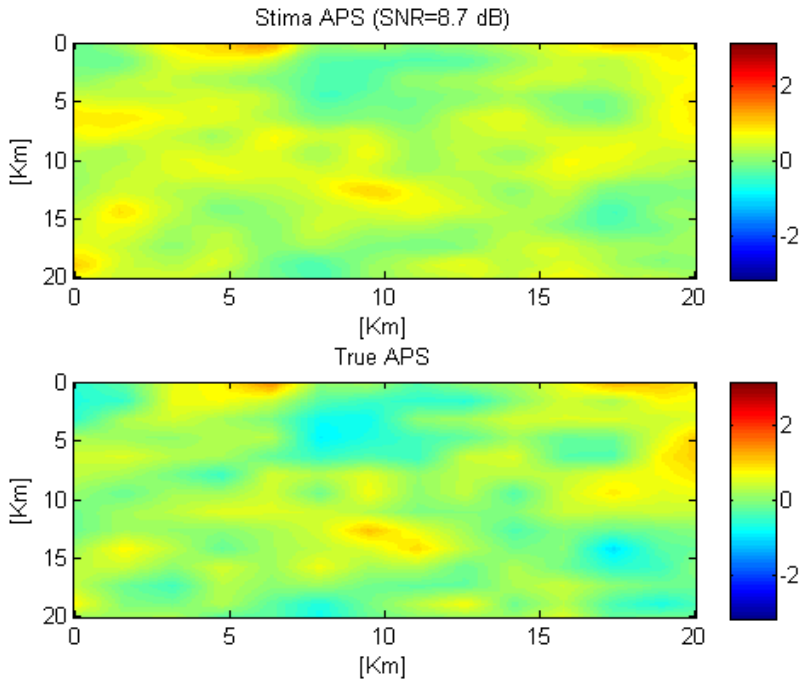

Figure 5.3: MLE: Estimate of the APS (above) with a SNR=8.7 dB, true APS (below)

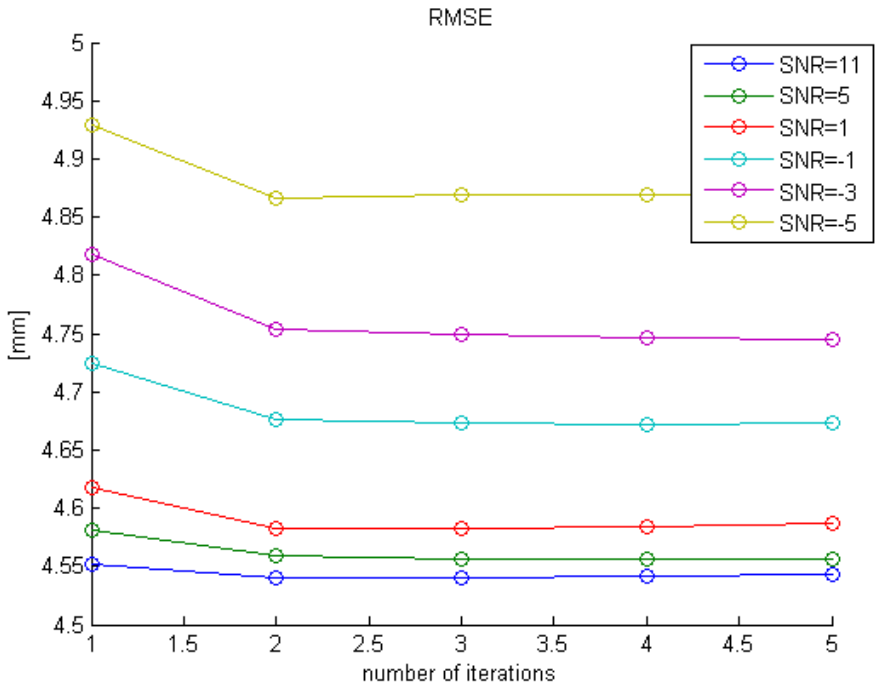

Figure 5.4: MLE: RMSE vs iterations

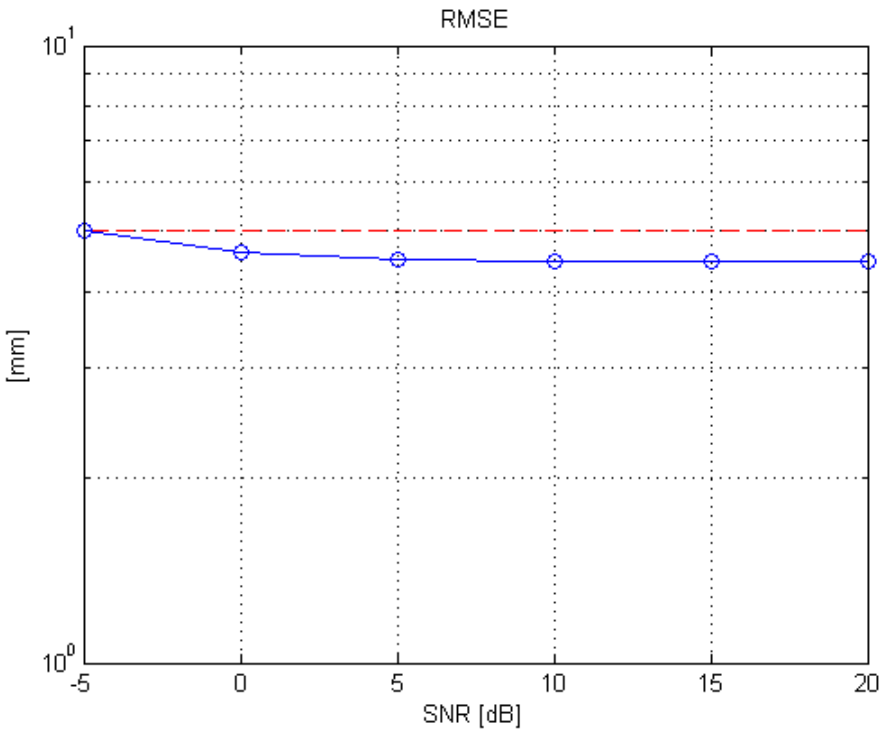

Figure 5.5: MLE: RMSE of the estimate of the APS after the second iteration(blue line), goal set at 5 mm (red dashed line).

In fig. 5.5 we may notice that the RMSE reaches a floor. The maximum likelihood should not behave in this way and the error should keep decreasing for higher SNR, but computing the derivatives in the system 5.7 we made an approximation (Appendix C, equation 7.31) that impacts the estimation of the atmospheric phase screen.

Chapter 6

Comparison of estimators

Now we want to compare the accuracy of the estimators presented (MMSE, SVD, MLE) to see which one performs better.

In fig.6.1 we can see the comparison of the RMSE of the estimators, it seems like the Singular Value Decomposition achieve better results, but the RMSE has been obtained assuming to know at one permanent scatterer per area, if this is not the case and we do not know enough PSs we have to estimate the APS in some areas using the overlapping of adjacent areas. This increases the error, the less PSs we know, the higher the RMSE, that can be as high as in fig.4.9 (if we know only one PS in the whole scene), where the RMSE is higher than any of the errors using other estimators.

Otherwise if we have a high SNR (in table 2.2 we stated that we expect a SNR of 8.7 dB) the best choice seems to be the MMSE after we estimated the scene through the average over many days. In fact with high SNR the average will yield good results, the residual error that is like noise added to the system will be minimal and then the MMSE is the best estimator at minimizing the error. If the SNR is low then the error of the average will be high and that will impact the RMSE of the APS too much. In addition the average and MMSE requires us to know the covariance of the APS (which we know from its autocorrelation

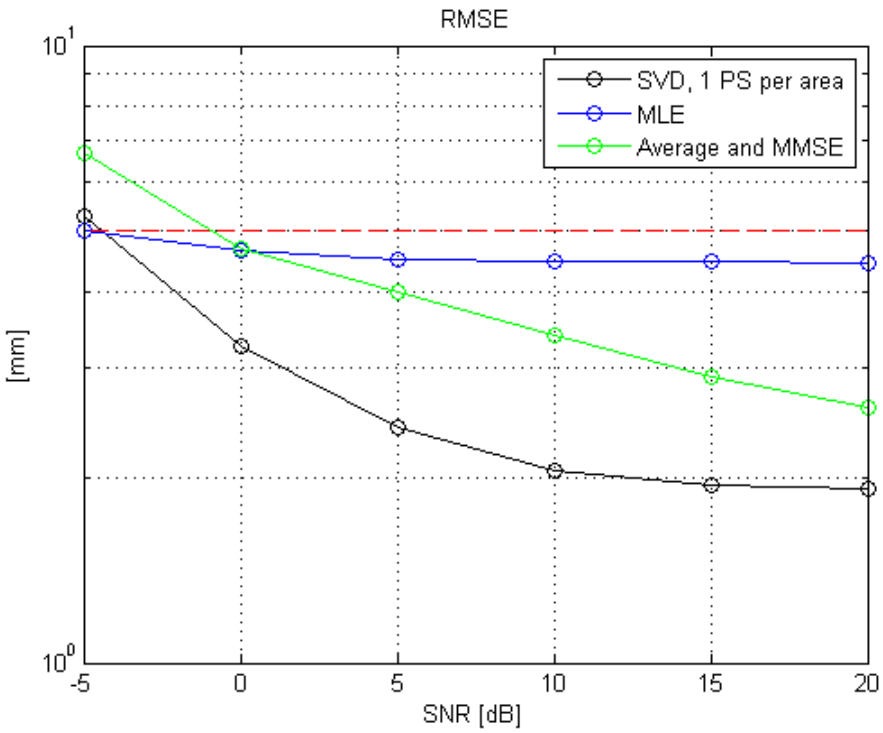

Figure 6.1: RMSE: comparison of the three different estimators presented in this thesis

function) and the covariance of the noise (which we might have to estimate).

The MLE seems to be the more resistant to noise so it is better with a low SNR, although it does not get a really good RMSE. As stated in chapter 7, the error reaches a floor because we made an approximation (Appendix C, equation 7.31).

In the end, in terms of RMSE, the SVD is the best choice if we have many permanent scatterers, otherwise the average and MMSE is better with higher SNR and the MLE with low SNR.

In terms of processing time the SVD and the MLE take about the same time, while the MMSE is slower because it requires the inversion of a matrix that might be quite big, depending on the size of the areas we use to divide the image.

In terms of memory used the MLE and the SVD are again similar, while the MMSE requires the storage of the covariance matrices of the atmospheric phase screen and the noise, that might be quite big.

Chapter 7

Conclusions

In this thesis we have started from the theory of synthetic aperture rader and then discussed the characteristics of a GEOSAR system, compared it to LEOSAR systems, introduced possible applications and presented the decorrelation issues that prevented the GOESAR to be implemented.

Among these problems we find the atmospheric phase screen, we showed its characteristics (variogram and autocorrelation function).

We presented three methods to estimate the phase distortion the APS introduces, starting from strong assumptions and then moved on to a more realistic scenario. The first method exploits the fact that the scene remains unchanged in consecutive days to estimate it through an average over many days. Then we removed it from the model and use an MMSE estimator to obtain the APS.

The second one exploit the fact that the model we used was a separable one to estimate the APS and the scene by means of a singular value decomposition.

In the last one we started from model and computed the maximum likelihood estimator.

In the end we showed a comparison of the results obtained using these methods.

Appendix A

Autocorrelation of the phase of the APS

As stated in equation 2.9 the autocorrelation function of the phase of the APS when there is no wrapping is

$$r(\tau, \chi) = e^{-\left(\frac{4\pi}{\lambda}\right)^2 \sigma_t^2 \sqrt{\left(\frac{\tau}{\tau_0}\right)^2 + \left(\frac{\chi}{\chi_0}\right)^2}}$$

If we take into account only time (with similar steps we can add the space dependence) in order to compute the autocorrelation we have to solve the following expected value

$$E\left[e^{-j\phi(t+\tau)} e^{j\phi(t)}\right]$$

this is equal to

$$E\left[e^{-j\frac{4\pi}{\lambda} d_{APS}(t+\tau)} e^{j\frac{4\pi}{\lambda} d_{APS}(t)}\right] = E\left[e^{j\frac{4\pi}{\lambda}(d_{APS}(t) - d_{APS}(t+\tau))}\right]$$

now using the property

$$E\left[e^{j\varphi}\right] = e^{\frac{\sigma_\varphi^2}{2}}$$

if we call

$$\varphi = \frac{4\pi}{\lambda}\left(d_{APS}(t) - d_{APS}(t+\tau)\right)$$

$$\sigma_\varphi^2 = var(\varphi) = \left(\frac{4\pi}{\lambda}\right)^2 var\left(d_{APS}(t) - d_{APS}(t+\tau)\right) = \left(\frac{4\pi}{\lambda}\right)^2 2V(\tau)$$

and using equation 2.2

$$\sigma_\varphi^2 = \left(\frac{4\pi}{\lambda}\right)^2 2\sigma_t^2 \left(1 - e^{\sqrt{\left(\frac{\tau}{\tau_0}\right)^2}}\right)$$

and since we will always work on the almost linear part of the variogram this can be further simplified

$$\sigma_\varphi^2 \cong \left(\frac{4\pi}{\lambda}\right)^2 2\sigma_t^2 \left|\frac{\tau}{\tau_0}\right|$$

and finally

$$r(\tau) = E\left[e^{j\varphi}\right] = E\left[e^{\frac{\sigma_\varphi^2}{2}}\right] \cong e^{-\left(\frac{4\pi}{\lambda}\right)^2 2\sigma_t^2 \left|\frac{\tau}{\tau_0}\right|}$$

With similar steps we can add the space dependence end obtain

$$r(\tau) \cong e^{-\left(\frac{4\pi}{\lambda}\right)^2 2\sigma_t^2 \sqrt{\left(\frac{\tau}{\tau_0}\right)^2 + \left(\frac{\chi}{\chi_0}\right)^2}}$$

Appendix B

Formulas for the power budget

For a radar system, targets are all the objects that reflect an electromagnetic wave. Each target is characterized by the radar cross section (RCS, σ), a complex coefficient that defines the target reflection at a certain frequency and polarization and depends on the view angles of the radar. Targets can divided in two categories: point and distributed targets.

We define a target as a point target when in a resolution cell the energy reflected comes from a single point that prevails over other nearby possible targets (a scatterer has a much higher RCS than every other point in the resolution cell).

For example a mirror (with area A) directed to the antenna might act a a point target and will backscatter most of the energy that illuminates it, the perceived RCS will be

$$\sigma_0 = \frac{4\pi A^2}{\lambda^2} \tag{7.1}$$

We talk about distributed target when there are several scatterers in the resolution cell and no one prevails over the others. If we consider to have N scatterers, everyone will have a RCS like

$$RCS(n) = \sigma_n e^{j\varphi_n} \qquad n = 1, \ldots, N \tag{7.2}$$

where σ_n will be similar for each scatterer since no one prevails.

If we call $s_R(k)$ the sum of the contributions of the N scatterers to the k^{th} pixel

$$s_R(k) = \sum_{i=1}^{N} \sigma_i e^{j\varphi_i} \tag{7.3}$$

The radar will sense a total RCS that is the superposition of the N scatterers and can be seen as a random walk

$$E\left[s_R(k)\right] = E\left[\sum_{i=1}^{N} \sigma_i e^{j\varphi_i}\right] = 0 \tag{7.4}$$

$$\begin{aligned} E\left[s_R(k)s_R^*(k)\right] &= E\left[\sum_{i=1}^{N}\sum_{k=1}^{N} \sigma_i\sigma_k e^{j(\varphi_i-\varphi_k)}\right] = \\ &= \sum_{i=1}^{N} E\left[\sigma_i^2\right] = N \cdot E\left[\sigma_i^2\right] \end{aligned} \tag{7.5}$$

It is a zero mean random process with standard deviation proportional to the number of scatterers in the resolution cell, the backscatter coefficient will be

$$\sigma_0 = E\left[\sigma_i^2\right] = \frac{E\left[s_R(k)s_R^*(k)\right]}{N} = \frac{\sigma_{s_R}^2}{N} \tag{7.6}$$

We can get the received power from the radar equation

$$P_R = \frac{P_T G_T}{4\pi r_0^2}\sigma_0 \frac{1}{4\pi r_0^2} A_R \tag{7.7}$$

where P_T is the transmitted power, G_T the antenna gain, r_0 the slant range, σ_0 the reflectivity of the target and A_R the effective area of the receiving antenna. Using the formula that links the effective area to the gain

$$A_R = G_R \frac{\lambda^2}{4\pi} \tag{7.8}$$

and since we are in a monostatic scenario $G_R = G_T = G$, we can rewrite equation 7.7 in the following way

$$P_R = \frac{P_T G^2 \lambda^2}{(4\pi)^3 r_0^4}\sigma_0 \tag{7.9}$$

All the targets are distributed over a surface S, so we can write the backscatter coefficient like

$$\sigma_0 = \sigma_{0,s} S \tag{7.10}$$

If we consider a rectangular antenna with size $L_a \times L_b$, we can write the received power like

$$P_R = \frac{P_T \left(L_a L_b\right)^2 \eta_2}{4\pi\lambda^2 r_0^4} \sigma_{0,s} S \tag{7.11}$$

where η_2 accounts for the two way overall losses.

The surface that contributes to the scattering is

$$S = \frac{c}{2\sin(\theta_I)} T_c \Delta\psi r_0 = \frac{c}{2\sin(\theta_I)} T_c \frac{\lambda}{L_a} r_0 \tag{7.12}$$

where T_c is the duration of the transmitted pulse and $\Delta\psi$ is the azimuth antenna aperture.

We can finally write the received power like

$$P_R = \frac{P_T \left(L_a L_b\right)^2 \eta_2}{4\pi\lambda^2 r_0^4} \sigma_{0,s} \frac{c}{2\sin(\theta_I)} T_c \frac{\lambda}{L_a} r_0 \tag{7.13}$$

The power spectral density (PSD) of the noise will be

$$N_0 = K T_0 F \tag{7.14}$$

where K is the boltzmann constant, T_0 is the reference temperature and F is the noise figure of the device.

The SNR will be given by

$$SNR = \frac{P_R}{N_0 B} \tag{7.15}$$

where B is the used bandwidth.

Therefore substituting equation 7.13 in 7.15 and rearranging the terms

$$SNR = P_M \left(\frac{G^2 \lambda^2 \eta_2}{(4\pi)^3 r_0^4} \right) \left(\sigma_{0,s} \frac{c}{2B \sin(\theta_I)} \frac{L_a}{2} \right) \left(\frac{T_S}{N_0} \right) \tag{7.16}$$

The first term is the average power, that is the product of the peak power and the duty cycle ($P_M = P_T d_c = P_T T_c f_{prf}$), the second term is the effect of the antenna gain, spherical divergency and total losses, the third term is the radar cross section of the targets (product of σ_0, ground resolution and azimuth resolution), the last term is the noise power in the extent of the matched filter, that is the duration of the synthetic aperture $T_S = \frac{\lambda r_0}{v L_a}$.

Appendix C
Derivation of MLE for APS estimation

Starting from the following model

$$y(p,d) = a(p)e^{j\frac{4\pi}{\lambda}d_{APS}(p,d)} + w(p,d) = \hat{y}(p,d) + w(p,d) \tag{7.17}$$

assuming to have a zero mean gaussian noise with covariance $\boldsymbol{C}_w$, the probability density function ($f(\boldsymbol{y}|\boldsymbol{a},\boldsymbol{\phi}_{APS})$) will be gaussian

$$f(\boldsymbol{y}|\boldsymbol{a},\boldsymbol{\phi}_{APS}) = \frac{1}{\sqrt{(2\pi)^{N_pN_d}\left|\boldsymbol{C}_w\right|}} exp\left(-\frac{1}{2}\left(\boldsymbol{y}-\hat{\boldsymbol{y}}(\boldsymbol{a},\boldsymbol{\phi}_{APS})\right)^H \boldsymbol{C}_w^{-1}\left(\boldsymbol{y}-\hat{\boldsymbol{y}}(\boldsymbol{a},\boldsymbol{\phi}_{APS})\right)\right) \tag{7.18}$$

Now we have to find the values of $a(p)$ and $\phi_{APS}(p,d)$ that maximaze the previous pdf

$$\boldsymbol{a},\boldsymbol{\phi}_{APS} = \arg\max_{\boldsymbol{a},\boldsymbol{\phi}_{APS}} \left\{f(\boldsymbol{y}|\boldsymbol{a},\boldsymbol{\phi}_{APS})\right\} \tag{7.19}$$

Looking at the log-form of the pdf in equation 7.18

$$\begin{aligned}\ln\left[f(\boldsymbol{y}|\boldsymbol{a},\boldsymbol{\phi}_{APS})\right] &= -\frac{N_pN_d}{2}\ln(2\pi) - \frac{1}{2}\ln\left(\left|\boldsymbol{C}_w\right|\right) + \\ &\quad -\frac{1}{2}\left(\boldsymbol{y}-\hat{\boldsymbol{y}}(\boldsymbol{a},\boldsymbol{\phi}_{APS})\right)^H \boldsymbol{C}_w^{-1}\left(\boldsymbol{y}-\hat{\boldsymbol{y}}(\boldsymbol{a},\boldsymbol{\phi}_{APS})\right)\end{aligned} \tag{7.20}$$

the first two terms are two constants, we have to maximize the third term. Looking at the third term we can neglect the $\frac{1}{2}$ constant and since there is a minus sign we can look for the minimum of

$$\boldsymbol{a}, \boldsymbol{\phi}_{APS} = \arg \min_{\boldsymbol{a}, \boldsymbol{\phi}_{APS}} \left\{ (\boldsymbol{y} - \hat{\boldsymbol{y}}(\boldsymbol{a}, \boldsymbol{\phi}_{APS}))^H \boldsymbol{C}_w^{-1} (\boldsymbol{y} - \hat{\boldsymbol{y}}(\boldsymbol{a}, \boldsymbol{\phi}_{APS})) \right\} \tag{7.21}$$

We can call the argument to be minimized $g(\boldsymbol{a}, \boldsymbol{\phi}_{APS})$, that will be

$$g(\boldsymbol{a}, \boldsymbol{\phi}_{APS}) = (\boldsymbol{y} - \hat{\boldsymbol{y}}(\boldsymbol{a}, \boldsymbol{\phi}_{APS}))^H \boldsymbol{C}_w^{-1} (\boldsymbol{y} - \hat{\boldsymbol{y}}(\boldsymbol{a}, \boldsymbol{\phi}_{APS})) \tag{7.22}$$

and this will be equal to

$$g(\boldsymbol{a}, \boldsymbol{\phi}_{APS}) = \sum_{p=1}^{N_p} \sum_{d=1}^{N_d} \left[\left(y(p,d) - a(p) e^{j\phi_{APS}(p,d)} \right)^* \frac{1}{\sigma_w^2} \left(y(p,d) - a(p) e^{j\phi_{APS}(p,d)} \right) \right] \tag{7.23}$$

and after multiplying the terms together

$$\begin{aligned} g(\boldsymbol{a}, \boldsymbol{\phi}_{APS}) \quad = \quad & \sum_{p=1}^{N_p} \frac{N_d \left| a(p) \right|^2}{\sigma_w^2} + \frac{1}{\sigma_w^2} \sum_{p=1}^{N_p} \sum_{d=1}^{N_d} \left| y(p,d) \right|^2 + \\ & + \frac{1}{\sigma_w^2} \sum_{p=1}^{N_p} \sum_{d=1}^{N_d} \left[y^*(p,d) a(p) e^{j \frac{4\pi}{\lambda} d_{APS}(p,d)} \right] + \\ & - \frac{1}{\sigma_w^2} \sum_{p=1}^{N_p} \sum_{d=1}^{N_d} \left[y(p,d) a^*(p) e^{-j \frac{4\pi}{\lambda} d_{APS}(p,d)} \right] \end{aligned} \tag{7.24}$$

Now we have to minimize $g(\boldsymbol{a}, \boldsymbol{\phi}_{APS})$, so we have to compute the derivatives w.r.t $a(p)$ and $d_{APS}(p,d)$ and set them to zero

$$\begin{cases} \frac{\partial}{\partial a(p)^*} g(\boldsymbol{a}, \boldsymbol{\phi}_{APS}) = 0 \\ \frac{\partial}{\partial d_{APS}(p,d)} g(\boldsymbol{a}, \boldsymbol{\phi}_{APS}) = 0 \end{cases} \tag{7.25}$$

The derivative w.r.t $a(p)$ is really simple to be computed and it yields

$$\frac{N_d a(p)}{\sigma_w^2} - \frac{1}{\sigma_w^2}\sum_{d=1}^{N_d} y(p,d)e^{-j\frac{4\pi}{\lambda}d_{APS}(p,d)} = 0$$

$$\hat{a}(p) = \frac{1}{N_d}\sum_{d=1}^{N_d} y(p,d)e^{-j\frac{4\pi}{\lambda}d_{APS}(p,d)} \tag{7.26}$$

The derivative w.r.t $d_{APS}(p,d)$ requires a bit more steps, we will get

$$\frac{1}{\sigma_w^2}\sum_{p=1}^{N_p}\left[-j\frac{4\pi}{\lambda}y^*(p,d)a(p)e^{j\phi_{APS}(p,d)} + j\frac{4\pi}{\lambda}y(p,d)a^*(p)e^{-j\phi_{APS}(p,d)}\right] = 0 \tag{7.27}$$

where, after simplifying for the constants $\frac{1}{\sigma_w^2}$ and $j\frac{4\pi}{\lambda}$, we can recognize the difference of two complex conjugate numbers. Using the property

$$z - z^* = 2j\text{Im}\{z\} \tag{7.28}$$

we can rewrite equation 7.27 like

$$\sum_{p=1}^{N_p} 2j\text{Im}\left\{y^*(p,d)a(p)e^{j\phi_{APS}(p,d)}\right\} = 0 \tag{7.29}$$

after we simplify the $2j$ constant, if we call

$$\begin{cases} a(p) = b + jc \\ y(p,d) = d + je \\ \phi_{APS}(p,d) = \varphi \end{cases}$$

we can rewrite equation 7.29 like

$$\text{Im}\left\{\sum_{p=1}^{N_p}(b+jc)(d-je)\left(\cos(\varphi) + j\sin(\varphi)\right)\right\} = 0$$

$$\text{Im}\left\{\sum_{p=1}^{N_p}\left(bd + ce + j\left(cd - be\right)\right)\left(\cos(\varphi) + j\sin(\varphi)\right)\right\} = 0$$

$$\sum_{p=1}^{N_p} \left[(cd - be)\cos(\varphi) + (bd + ce)\sin(\varphi)\right] = 0$$

$$\sum_{p=1}^{N_p} \left[(bd + ce)\sin(\varphi)\right] = \sum_{p=1}^{N_p} \left[(be - cd)\cos(\varphi)\right] \tag{7.30}$$

Now if we assume the APS to have a constant value over points ($\tilde{p}$) close to each other ($\tilde{p} = 1, \ldots, \tilde{N}_p$ with $\tilde{N}_p \ll N_p$), we can take $\sin(\varphi)$ and $\cos(\varphi)$ out of the summation

$$\sin(\varphi) \sum_{\tilde{p}=1}^{\tilde{N}_p} (bd + ce) = \cos(\varphi) \sum_{\tilde{p}=1}^{\tilde{N}_p} (be - cd)$$

$$\tan(\varphi) = \frac{\sum_{\tilde{p}=1}^{\tilde{N}_p} (be - cd)}{\sum_{\tilde{p}=1}^{\tilde{N}_p} (bd + ce)} \tag{7.31}$$

and finally we get the solution to the derivative w.r.t d_{APS}

$$\hat{\phi}_{APS}(p, d) = tan^{-1} \left(\frac{\sum_{\tilde{p}=1}^{\tilde{N}_p} \left[\mathrm{Re}\{a(\tilde{p})\}\mathrm{Im}\{y(\tilde{p}, d)\} - \mathrm{Im}\{a(\tilde{p})\}\mathrm{Re}\{y(\tilde{p}, d)\}\right]}{\sum_{\tilde{p}=1}^{\tilde{N}_p} \left[\mathrm{Re}\{a(\tilde{p})\}\mathrm{Re}\{y(\tilde{p}, d)\} - \mathrm{Im}\{a(\tilde{p})\}\mathrm{Im}\{y(\tilde{p}, d)\}\right]} \right) \tag{7.32}$$

Now that we have computed the two derivatives in equation 7.25 we have the maximum likelihood estimator, which is the following system

$$\begin{cases} \hat{a}(p) = \frac{1}{N_d} \sum_{d=1}^{N_d} y(p, d) e^{-j \frac{4\pi}{\lambda} d_{APS}(p,d)} \\ \hat{\phi}_{APS}(p, d) = tan^{-1} \left(\frac{\sum_{\tilde{p}=1}^{\tilde{N}_p} [\mathrm{Re}\{a(\tilde{p})\}\mathrm{Im}\{y(\tilde{p},d)\} - \mathrm{Im}\{a(\tilde{p})\}\mathrm{Re}\{y(\tilde{p},d)\}]}{\sum_{\tilde{p}=1}^{\tilde{N}_p} [\mathrm{Re}\{a(\tilde{p})\}\mathrm{Re}\{y(\tilde{p},d)\} - \mathrm{Im}\{a(\tilde{p})\}\mathrm{Im}\{y(\tilde{p},d)\}]} \right) \end{cases} \tag{7.33}$$

Bibliography

[1] Andrea Monti Guarnieri. *Introduction to RADAR*. 2003.

[2] `http://www.cosmo-skymed.it/it/index.htm`.

[3] `https://sentinel.esa.int/web/sentinel/missions/sentinel-1`.

[4] K. Tomiyasu. Synthetic aperture radar in geosynchronous orbit. *IEEE Antenna Propagation Society Symposium*, 1978.

[5] D. Bruno and Hobbs S. E. Radar imaging from geosynchronous orbit: temporal decorrelation aspects. *IEEE Transactions on geoscience and remote sensing*, 2010.

[6] S.N. Madsen, W. Edelstein, L.D. Di Domenico, and J. La Breque. A geosynchronous synthetic aperture radar for tectonic mapping, disaster management and measurements of vegetation and soil moisture. *IEEE Transactions on geoscience and remote sensing*, 2001.

[7] A Ferretti, C. Prati, and F. Rocca. Nonlinear subsidence rate estimation using permanent scatterers in differential sar interferometry. *IEEE Transactions on geoscience and remote sensing*, 2000.

[8] A. Monti Guarnieri, F. Rocca, and A. Broquetas. Impact of atmospheric water vapor on the design of a ku band geosynchronous sar system. *IEEE Transactions on geoscience and remote sensing*, 2009.

[9] W.J. Qu, W.Y. Zhu, S.L. Song, and J.S. Ping. Evaluation of the precision of three tropospheric delay correction models. *Chinese astronomy and astrophysics*, 2008.

[10] L. Iannini and A. Monti Guarnieri. Atmospheric phase screen in ground-based radar: statistics and compensation. *IEEE Transactions on geoscience and remote sensing*, 2011.

[11] S. Hobbs, C. Mitchell, B. Forte, R Holley, B. Snapir, and P. Whittaker. System design for geosynchronous synthetic aperture radar missions. *IEEE Transactions on geoscience and remote sensing*, 2014.

[12] J. Ruiz Rodon, A. Broquetas, A. Monti Guarnieri, and F. Rocca. Geosynchronous sar focusing with atmospheric phase screen retrival and compression. *IEEE Transactions on geoscience and remote sensing*, 2013.

[13] L. Perletta and D. Scapin. *Thesis: Progetto di un sistema SAR geosincrono ad alta risoluzione: stima e compensazione dello schermo atmosferico di fase.* 2012.

[14] A. Monti Guarnieri, A. Recchia, A. Broquetas, and J. Ruiz-Rodon. Assesment of atmospheric phase screen impacts and statistics in view of future geosynchronous sar missions. *Igarss 2014*, 2014.

[15] `http://www.esa.int/spaceinimages/Images/2014/09/Po_Valley_Italy`.

[16] P. Guccione, A. Monti Guarnieri, and S. Tebaldini. Stable target detection and coherence estimation in interferometric sar stacks. *IEEE Transactions on geoscience and remote sensing*, 2012.